ARTICLE

Check for updates

Glial type specific regulation of CNS angiogenesis by HIFα-activated different signaling pathways

Sheng Zhang [1,2,5], Bokyung Kim [1,2,5], Xiaoqing Zhu[1,4], Xuehong Gui[1], Yan Wang[1,2], Zhaohui Lan[1,2], Preeti Prabhu[1], Kenneth Fond[1], Aijun Wang [1,3] & Fuzheng Guo [1,2✉]

The mechanisms by which oligodendroglia modulate CNS angiogenesis remain elusive. Previous in vitro data suggest that oligodendroglia regulate CNS endothelial cell proliferation and blood vessel formation through hypoxia inducible factor alpha (HIFα)-activated Wnt (but not VEGF) signaling. Using in vivo genetic models, we show that HIFα in oligodendroglia is necessary and sufficient for angiogenesis independent of CNS regions. At the molecular level, HIFα stabilization in oligodendroglia does not perturb Wnt signaling but rather activates VEGF. At the functional level, genetically blocking oligodendroglia-derived VEGF but not Wnt significantly decreases oligodendroglial HIFα-regulated CNS angiogenesis. Blocking astroglia-derived Wnt signaling reduces astroglial HIFα-regulated CNS angiogenesis. Together, our in vivo data demonstrate that oligodendroglial HIFα regulates CNS angiogenesis through Wnt-independent and VEGF-dependent signaling. These findings suggest an alternative mechanistic understanding of CNS angiogenesis by postnatal glial cells and unveil a glial cell type-dependent HIFα-Wnt axis in regulating CNS vessel formation.

[1] Institute for Pediatric Regenerative Medicine, Shriners Hospitals for Children/UC Davis School of Medicine, Sacramento, CA 95817, USA. [2] Department of Neurology, School of Medicine, UC Davis, Sacramento, CA 95817, USA. [3] Department of Surgery, School of Medicine, UC Davis, Sacramento, CA 95817, USA. [4] Present address: Qingdao University, Qingdao, China. [5] These authors contributed equally: Sheng Zhang, Bokyung Kim. ✉email: fzguo@ucdavis.edu

The vasculature of the central nervous system (CNS), which is developed exclusively through angiogenesis, plays a crucial role in providing neural cells with nutrients and oxygen. CNS angiogenesis, the growth of new blood vessels from pre-existing ones, starts during embryonic development and matures during postnatal development in human and rodent brains, for example, by the age of one month in rodents[1]. Dysregulated CNS angiogenesis negatively impacts postnatal brain development and functional recovery from brain injuries[2–4]. The current study aimed to dissect the molecular regulation of postnatal CNS angiogenesis using in vivo genetic animal models.

The developing CNS parenchyma is exposed to physiological hypoxia with local oxygen concentration ranging from 0.5 to 7%[5]. Hypoxia-inducible factor α (HIFα) is a critical regulator that adapts neural cells to hypoxic conditions. The transcription factor HIFα, including HIF1α and HIF2α, is subjected to constant degradation. Von Hippel-Lindau (VHL), a negative regulator of HIFα's transcriptional activity, plays an essential role in HIFα degradation. Under low oxygen or upon VHL disruption, HIF1α and HIF2α degradation is impaired and subsequently translocate into the nuclei where they regulate downstream target genes through forming transcriptional active complexes with the constitutive HIF1β[6,7]. Previous data suggest that HIFα function in neural precursor cells is required for embryonic brain vascular development[8]. Recent data including those from our own laboratory show that HIFα function in oligodendroglial lineage cells may play a pivotal role in regulating postnatal angiogenesis in the brain white matter[9] and in the spinal cord[10]. However, the molecular mechanisms underlying oligodendroglial HIFα-regulated angiogenesis are still controversial and remain incompletely defined.

The current concept stated that oligodendroglial HIFα promotes CNS angiogenesis through activating signaling pathway of Wnt but not vascular endothelial growth factor (VEGF)[9]. However, this "Wnt-dependent" view was supported only by in vitro studies and pharmacological manipulations[9], in which "pathological" activation of Wnt signaling, poor cell-type selectivity and/or off-target effects of small compounds cannot be excluded. In this study, we present in vivo evidence supporting an alternative view in our mechanistic understanding of oligodendroglial HIFα-regulated CNS angiogenesis. Our in vivo genetic knockout data reveal that oligodendroglial HIFα regulates endothelial cell proliferation and angiogenesis in a VEGF-dependent but Wnt-independent manner and this regulation is independent of CNS regions during postnatal development. This data also demonstrate that postnatal astroglia regulate CNS angiogenesis at least in part through HIFα-activated Wnt signaling, unveiling a glial cell type-specific HIFα-Wnt connection in the CNS.

Results

Oligodendroglial HIFα regulates CNS angiogenesis. Endothelial cell (EC) proliferation is an essential step of angiogenesis and the blood vessel density is an end-point reflection of angiogenesis. Therefore, we used EC proliferation and vessel density as in vivo readouts of angiogenesis[9]. To quantify blood vessel density, we used the basement membrane marker Laminin to label blood vessels and employed a semi-automated approach to calculate the percentage of Laminin-occupying area among total assessed area (Supplementary Fig. 1). To determine whether oligodendroglial HIFα is required for angiogenesis throughout the postnatal CNS, Cre-LoxP approach was used to genetically ablate or stabilize HIFα and EC proliferation and vessel density were analyzed in the brain and the spinal cord.

We used *Cnp-Cre* line[11] to generate *Cnp-Cre:Hif1α*^{fl/fl} (HIF1α conditional knockout, cKO), *Cnp-Cre: Hif2α*^{fl/fl} (HIF2α cKO),

and *Cnp-Cre: Hif1α*^{fl/fl}*:Hif2α*^{fl/fl} (HIF1α/HIF2α or HIFα double cKO) mutants (Supplementary Fig. 2). Mice carrying Cnp-Cre transgene alone did not display any developmental abnormalities compared with non-Cre animals as previously reported[11] and supported by our assessment of CNS angiogenesis at postnatal 10 and motor function at postnatal one month (Supplementary Fig. 3). HIF1α cKO or HIF2α cKO did not influence blood vessel density, indicating a compensatory effect of oligodendroglial HIF1α and HIF2α on angiogenesis. In contrast, HIF1α/HIF2α double cKO (refer to as HIFα cKO hereafter) significantly impaired CNS angiogenesis evidenced by reduced blood vessel density (Fig. 1a–c) and diminished EC proliferation not only in the cerebral cortex but also in the spinal cord at postnatal 14 (Fig. 1d–g), suggesting that oligodendroglial HIFα is necessary for CNS angiogenesis.

The HIFα protein is constantly translated but subjected to rapid turnover via proteasome-mediated degradation, a process in which Von Hippel-Lindau product (VHL) is essential for HIFα degradation. Therefore, we employed *Cnp-Cre:Vhl*^{fl/fl} transgenic mice to genetically ablate VHL and stabilize HIFα function in oligodendroglial lineage cells (Supplementary Fig. 4). We found that the density of blood vessels and the proliferation of ECs were significantly increased in the cerebral cortex and spinal cord of *Cnp-Cre:Vhl*^{fl/fl} mice compared with those of non-Cre control mice at different time points in the early postnatal CNS (Fig. 1h–j). Stabilizing HIFα in oligodendroglial lineage cells did not have a major effect on the integrity of the blood-brain (spinal cord) barrier in the adult *Cnp-Cre:Vhl*^{fl/fl} mice (Supplementary Fig. 5).
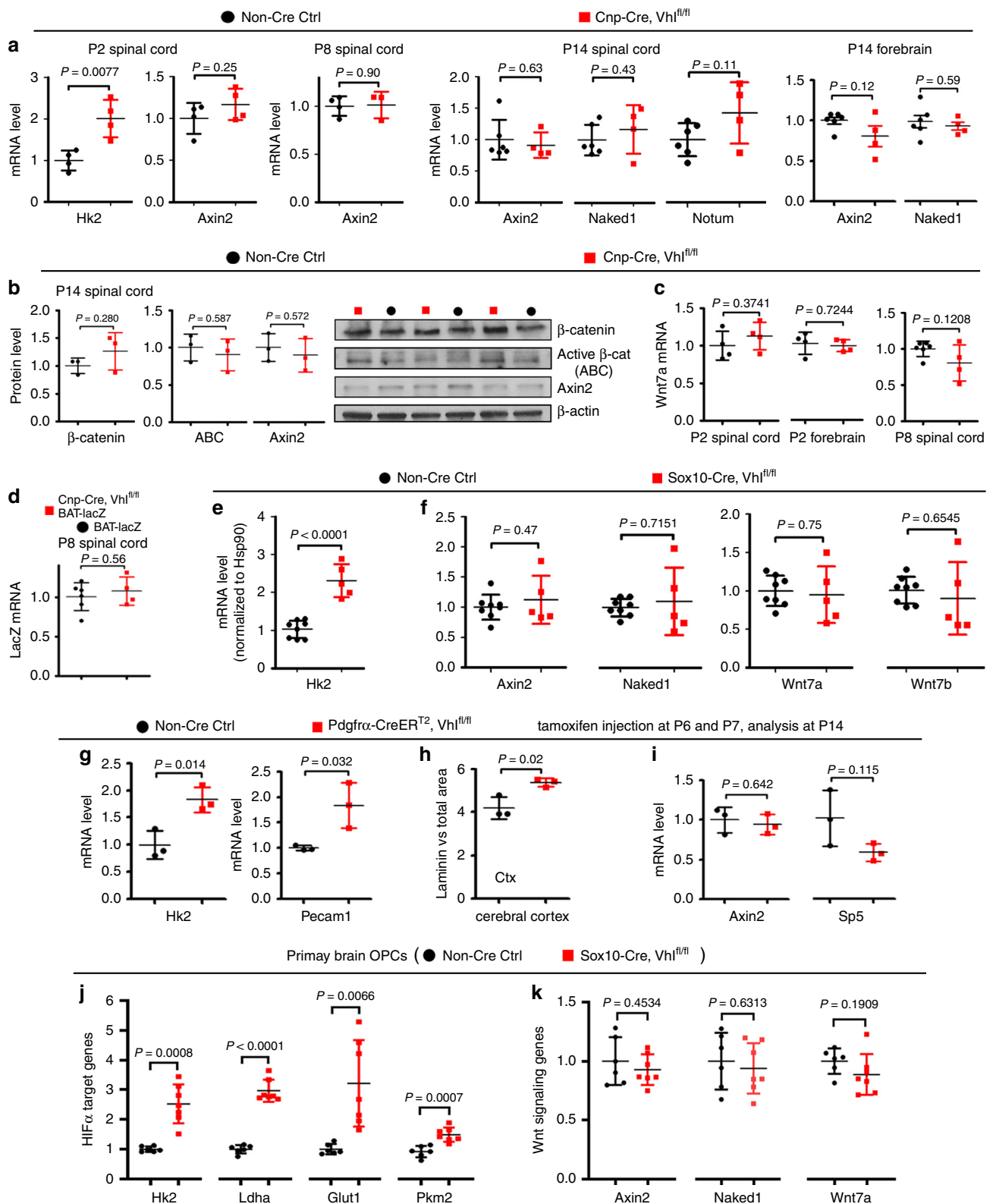
Previous studies have reported that *Cnp-Cre* primarily targets oligodendroglial lineage cells and also a subpopulation of early neural progenitor cells[12,13]. To corroborate the conclusion derived from Cnp-Cre transgenic mice, we assessed CNS angiogenesis in a different animal strain *Sox10-Cre:Vhl*^{fl/fl} in which *Sox10-Cre* mediated HIFα stabilization in the earlier stages of oligodendrocyte development in the CNS. Consistently, CNS angiogenesis was significantly increased in *Sox10-Cre:Vhl*^{fl/fl} mutants, as assessed by elevated blood vessel density (Fig. 1k), EC-specific Pecam1 mRNA expression (Fig. 1l), and EC densities (Fig. 1m). Taken together, our loss (gain)-of-function results suggest that oligodendroglial HIFα is necessary and sufficient for angiogenesis and that the angiogenic regulation by oligodendroglial HIFα is independent of CNS regions.

Oligodendroglial HIFα does not regulate Wnt signaling. To determine whether HIFα in oligodendroglial lineage cells regulates Wnt/β-catenin signaling, we quantified the Wnt/β-catenin target gene *Axin2*, *Naked1*, and *Notum*, which are reliable readouts for the signaling activation[10]. We found no significant changes in the mRNA levels of those genes in HIFα-stabilized spinal cord and forebrain of *Cnp-Cre:Vhl*^{fl/fl} mutants at different time points (Fig. 2a) compared with those of non-Cre controls. Consistently, western blot assay showed that the active form of β-catenin (dephosphorylated on Ser37 or Thr41) and Axin2 did not change (Fig. 2b), indicating that stabilizing oligodendroglial HIFα does not perturb the activity of Wnt/β-catenin signaling in the CNS. Furthermore, we found no significant change in the mRNA level of Wnt7a in the CNS of *Cnp-Cre:Vhl*^{fl/fl} mice compared with non-Cre controls (Fig. 2c). We crossed Wnt reporter transgenic mice BAT-lacZ[14] with *Cnp-Cre:Vhl*^{fl/fl} mutants and found no difference in lacZ mRNA level in the spinal cord of BAT-lacZ/*Cnp-Cre:Vhl*^{fl/fl} mice compared with age-matched BAT-lacZ mice (Fig. 2d).

We further assessed the activity of Wnt/β-catenin signaling in a different animal strain of *Sox10-Cre:Vhl*^{fl/fl} mice. Consistent with
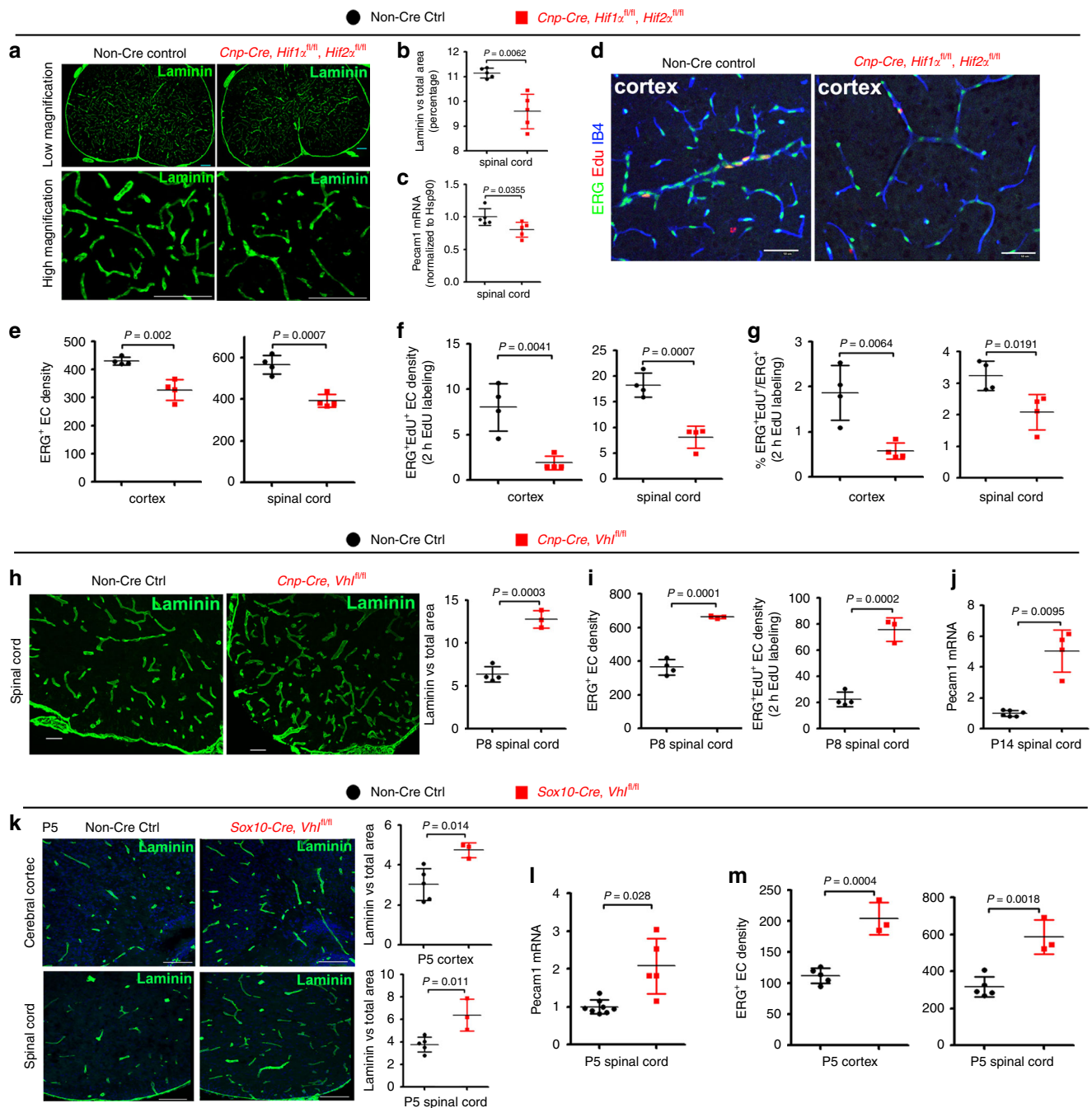
Fig. 1 CNS region-independent regulation of angiogenesis by oligodendroglial HIFα. a Representative images of blood vessels labeled by the basement membrane marker Laminin in the spinal cord of *Cnp-Cre:Hif1α*^{fl/fl}:*Hif2α*^{fl/fl} and non-Cre littermate controls at postnatal day 14 (P14). Scale bars = 100 μm. **b** Percentage of Laminin[+] area among total assessed area. Two-tailed Student's *t* test with Welch's correction, $t_{(4.618)} = 4.767$, $n = 5$ each group. **c** RT-qPCR assay of *Pecam1* mRNA (a.k.a. CD31), a marker of endothelial cells (ECs), in the P14 spinal cord. Two-tailed Student's *t* test, $t_{(8)} = 2.526$, $n = 5$ each group. **d–f** Representative images of immunohistochemical staining of ERG (a nuclear marker of ECs), isolectin B4 (IB4, labeling blood vessel basement membrane), and EdU (labeling actively dividing cells) and densities of marker positive cells (# per mm[2]) in *Cnp-Cre, Hif1α*^{fl/fl}, *Hif2α*^{fl/fl} and littermate control mice at P14. Two hours EdU pulse labeling. Two-tailed Student's *t* test, ERG[+], $t_{(6)} = 5.200$ cortex, $t_{(6)} = 6.358$ spinal cord; ERG[+]EdU[+], $t_{(6)} = 4.496$ cortex, $t_{(6)} = 6.365$ spinal cord. $n = 4$ each group. **g** Percentage of ERG[+] ECs that are EdU[+]. Two-tailed Student's *t* test, $t_{(6)} = 4.089$ cortex, $t_{(6)} = 3.181$ spinal cord. $n = 4$ each group. **h** Representative images and quantification of Laminin in the spinal cord of P8 *Cnp-Cre, Vhl*^{fl/fl}, and non-Cre control mice. Two-tailed Student's *t* test, $t_{(5)} = 8.831$. $n = 4$ Ctrl, 3 VHL cKO. **i** Densities (per mm[2]) of ERG[+] ECs and ERG[+]EdU[+] proliferating ECs in the P8 spinal cord. Two-tailed Student's *t* test, $t_{(5)} = 11.10$ ERG[+], $t_{(5)} = 9.981$ ERG[+]EdU[+]. $n = 4$ Ctrl, 3 VHL cKO. **j** RT-qPCR of *Pecam1* mRNA in P14 spinal cord. Two-tailed Student's *t* test with Welch's correction, $t_{(3.081)} = 5.941$. $n = 6$ Ctrl, 4 VHL cKO. **k** Representative images and quantification of Laminin in P5 *Sox10-Cre, Vhl*^{fl/fl} and non-Cre controls. Two-tailed Student's *t* test, $t_{(6)} = 3.625$ spinal cord, $t_{(6)} = 3.428$ cortex. $n = 5$ Ctrl, 3 VHL cKO. **l** RT-qPCR of *Pecam1* mRNA in P5 spinal cord. Two-tailed Student's *t* test with Welch's correction, $t_{(4.309)} = 3.257$. $n = 8$ Ctrl, 5 VHL cKO. **m** Densities (per mm[2]) of ERG[+] ECs at P5. Two-tailed Student's *t* test, $t_{(6)} = 6.964$ cortex, $t_{(6)} = 5.324$ spinal cord. $n = 5$ Ctrl, 3 VHL cKO. Scale bar: **a, k** 100 μm; **d, h** 50 μm. Data are shown as mean ± s.d. Source data of **b, c, e, m** are provided as a Source Data file.

conditional *Pdgfrα-CreER*^T2:*Vhl*^fl/fl strain in which *Pdgfrα-CreER*^T2 elicited a greater than 85% of recombination efficiency and specificity in early postnatal oligodendrocyte progenitor cells (OPCs) (Supplementary Fig. 7). Tamoxifen-induced VHL ablation in OPCs resulted in HIFα stabilization and elevated angiogenesis, as demonstrated by significant increase in the expression of HIFα target gene *Hk2* and EC-specific *Pecam1*

Fig. 2 Oligodendroglial HIFα does not activate Wnt/β-catenin signaling. a RT-qPCR assay of mRNA levels of HIFα target gene *Hk2* and Wnt/β-catenin target genes *Axin2*, *Naked1*, and *Notum*. Two-tailed Student's *t* test, $t_{(6)} = 3.936$ *Hk2*, $t_{(6)} = 1.275$ *Axin2* at P2; $t_{(5)} = 0.1307$ *Axin2* at P8; $t_{(8)} = 0.4906$ *Axin2*, $t_{(8)} = 0.8386$ *Naked1*, $t_{(8)} = 1.821$ *Notum* at P14 spinal cord; $t_{(8)} = 1.736$ *Axin2*, $t_{(8)} = 0.5617$ *Naked1* at P14 forebrain. $n = 6$ Ctrl, 4 VHL cKO. **b** Western blot assay of total β-catenin, active β-catenin, and Axin2. Two-tailed Student's *t* test, $t_{(4)} = 1.247$ β-catenin, $t_{(4)} = 0.5869$ active β-catenin, $t_{(4)} = 0.614$ Axin2. $n = 3$ each group. **c** RT-qPCR of Wnt7a mRNA. Two-tailed Student's *t* test, $t_{(6)} = 0.960$ P2 spinal cord, $t_{(6)} = 0.3724$ P2 forebrain, $t_{(8)} = 1.736$ P8 spinal cord. $n = 4$ each group at P2, $n = 6$ Ctrl, 4 VHL cKO at P8. **d** RT-qPCR of lacZ mRNA in Wnt/β-catenin reporter mice (BAT-lacZ) that had been crossed onto *Cnp-Cre, Vhl*fl/fl and non-Cre control backgrounds. Two-tailed Student's *t* test, $t_{(8)} = 0.6072$. $n = 6$ BAT-lacZ, 4 *Cnp-Cre,Vhl*fl/fl,BAT-lacZ. **e, f** RT-qPCR assay of mRNA level of Hk2, Axin2, Naked1, Wnt7a, and Wnt7b in the spinal cord of *Sox10-Cre:Vhl*fl/fl and non-Cre controls at P5. Two-tailed Student's *t* test, $t_{(11)} = 7.011$ *Hk2*, $t_{(11)} = 0.7422$ *Axin2*, Welch's corrected $t_{(4.345)} = 0.392$ *Naked1*, $t_{(11)} = 0.3216$ *Wnt7a*, Welch's corrected $t_{(4.709)} = 0.4827$ *Wnt7b*. $n = 8$ Ctrl, 5 VHL cKO. **g** RT-qPCR of HIFα target gene *Hk2* and EC marker *Pecam1* in P14 spinal cord. Two-tailed Student's *t* test, $t_{(4)} = 4.158$ *Hk2*, $t_{(4)} = 3.231$ *Pecam1*. $n = 3$ each group. **h** Percent of laminin-occupying area among total area in the cerebral cortex at P14. Two-tailed Student's *t* test, $t_{(4)} = 3.724$. $n = 3$ each group. **i** Expression of Wnt/β-catenin target gene *Axin2* and *Sp5* in the spinal cord at P14 quantified by RT-qPCR. Two-tailed Student's *t* test, $t_{(4)} = 0.5021$ *Axin2*, $t_{(4)} = 2.006$ *Sp5*. $n = 3$ each group. **j, k** RT-qPCR assay of mRNA levels of HIFα target genes and Wnt signaling genes in primary OPCs isolated from the neonatal brain of *Sox10-Cre, Vhl*fl/fl and non-Cre control mice. Two-tailed Student's *t* test, Welch's corrected $t_{(6.282)} = 6.065$ *Hk2*, Welch's corrected $t_{(7.898)} = 12.92$ *Ldha*, Welch's corrected $t_{(6.199)} = 4.009$ *Glut1*, $t_{(11)} = 4.654$ *Pkm2*, $t_{(11)} = 0.7772$ *Axin2*, $t_{(11)} = 0.4936$ *Naked1*, $t_{(11)} = 1.394$ *Wnt7a*. $n = 6$ Ctrl, 7 VHL cKO. Data are shown as mean ± s.d. Source data of **a**–**k** are provided as a Source Data file.

(Fig. 2g) and the density of cerebral blood vessels (Fig. 2h). However, the mRNA expression of Wnt target genes *Ainx2* and *Sp5* (Fig. 2i) and the protein levels of active β-catenin and Naked1 (Supplementary Fig. 8) were indistinguishable between *Pdgfrα-CreER*[T2]:*Vhl*fl/fl mutants and non-Cre controls, indicating that Wnt/β-catenin signaling activity was not altered by oligodendroglial HIFα stabilization.

Previous study reported an autocrine activation of Wnt/β-catenin signaling in OPCs by HIFα stabilization[9]. To assess the autocrine activity of Wnt/β-catenin signaling, we treated purified primary OPCs with HIFα stabilizer DMOG[9] in the presence or absence of HIFα signaling blocker Chetomin[15] (Supplementary Fig. 9a). Our results showed that pharmacological stabilizing HIFα activated HIFα signaling target genes (Supplementary Fig. 9b) but did not activate Wnt/β-catenin target genes nor Wnt7a and Wnt7b (Supplementary Fig. 9c) in primary OPCs isolated from neonatal brain. We also quantified the activity of Wnt/β-catenin signaling in primary OPCs which were isolated from neonatal *Sox10-Cre:Vhl*fl/fl brain. Consistent with the in vivo data (Fig. 2e), HIFα target genes were significantly increased in primary VHL-deficient OPCs (Fig. 2j). However, neither Wnt/β-catenin target genes Axin2 and Naked1 nor Wnt7a were increased in primary VHL-deficient OPCs (Fig. 2k), suggesting that stabilizing oligodendroglial HIFα does not perturb Wnt/β-catenin signaling in primary OPCs.

To determine whether HIFα deletion affects Wnt/β-catenin signaling, we analyzed Wnt/β-catenin activity in the early postnatal CNS of Cnp-Cre:HIFα cKO and Pdgfrα-CreER[T2]:HIFα cKO mutants. Consistent with HIFα-stabilized mutants (Fig. 2), we found no evidence of Wnt/β-catenin signaling perturbation in both strains of HIFα cKO mutants (Supplementary Fig. 10). Collectively, our in vivo and in vitro data demonstrate that Wnt/β-catenin signaling is unlikely a downstream target of oligodendroglial HIFα as previously reported[9] and suggest that oligodendroglial HIFα may regulate CNS angiogenesis independent of Wnt/β-catenin signaling.

OPC autocrine Wnt signaling is dispensable for angiogenesis. WLS is an essential factor of Wnt secretion from Wnt-producing cells and its deficiency blocks Wnt ligands from activating the downstream pathways in Wnt-receiving cells[16–19]. To determine whether WLS deficiency affects Wnt secretion from oligodendroglial lineage cells, we knocked down WLS in primary Wnt7a-expressing OPCs and assessed Wnt secretion and autocrine Wnt/β-catenin activity (Fig. 3a, b). Because Wnt7a has been shown as one of the major Wnt ligand genes expressed in OPCs at the mRNA level[9,20], we overexpressed Wnt7a in primary OPCs.

Our enzyme-linked immunosorbent assay (ELISA) of the culture medium showed that WLS knockdown significantly reduced Wnt7a concentration secreted from Wnt7a-expressing OPCs (Fig. 3c). Autocrine Wnt/β-catenin signaling was activated in Wnt7a-expressing OPCs, as evidenced by the increased expression of Wnt target genes Axin2 and Sp5 (Fig. 3d), but this activation was blocked in WLS-deficient OPCs (Fig. 3d). Our data suggest that WLS is required for Wnt secretion from OPCs.

To define the putative in vivo role of Wnt signaling in HIFα-regulated CNS angiogenesis, we generated VHL/WLS double mutant hybrids to block Wnt secretion from HIFα-stabilized oligodendroglial lineage cells (Fig. 4a). Because constitutive *Sox10-Cre:Vhl*fl/fl pups died at very early postnatal ages, we used an inducible Cre line *Sox10-CreER*[T2] to stabilize HIFα and disrupt WLS (Fig. 4b, c) in Sox10^{+} oligodendroglial lineage cells (OPCs and differentiated oligodendroglia). Our fate-mapping data showed that *Sox10-CreER*[T2] elicited ~60% of recombination efficiency and greater than 90% of oligodendroglial specificity in Sox10^{+} oligodendroglial lineage cells in the early postnatal CNS (Supplementary Fig. 11). We confirmed that HIFα's function was indeed stabilized in the spinal cord of *Sox10-CreER*[T2]:*Vhl*fl/fl (HIFα-stabilized mice) and *Sox10-CreER*[T2]:*Vhl*fl/fl:*Wls*fl/fl (HIFα-stabilized/WLS-disrupted mice), as evidenced by the elevated expression of HIFα target gene *Hk2* (Fig. 4d) and *Ldha* (Fig. 4e) in comparison with non-Cre controls. Our analysis demonstrated that blocking Wnt secretion by disrupting WLS did not alter HIFα stabilization-elicited CNS angiogenesis in HIFα-stabilized/WLS-disrupted mice compared with HIFα-stabilized mice, which was supported by unchanged levels of endothelial *Pecam1* mRNA expression (Fig. 4f) and unchanged densities of blood vessels (Fig. 4g–j), ERG[+] ECs (Fig. 4k), and ERG[+]EdU[+] dividing ECs (Fig. 4l) in the spinal cord and cerebral cortex of HIFα-stabilized/WLS-disrupted mice compared with those of HIFα-stabilized mice. These data suggest that oligodendroglial lineage-derived Wnt signaling plays a minor role in HIFα-regulated angiogenesis in the early postnatal CNS.

Next, we used a different Cre transgenic line *Pdgfrα-CreER*[T2] to stabilize HIFα specifically in OPCs. OPC-specific HIFα stabilization enhanced blood vessel density (Fig. 5a–d) and increased the number of ERG[+] ECs (Fig. 5e, f) in the spinal cord and cerebral cortex of *Pdgfrα-CreER*[T2]:*Vhl*fl/fl animals compared with those in non-Cre controls. However, blocking Wnt secretion from OPCs by disrupting WLS did not affect blood vessel formation and endothelial cell density in the CNS of HIFα stabilized/WLS-disrupted mice compared with HIFα stabilized mice (*Pdgfrα-CreER*[T2]:*Vhl*fl/fl:*Wls*fl/fl versus *Pdgfrα-CreER*[T2]:*Vhl*fl/fl) (Fig. 5c–f). The data from two independent Cre transgenic lines collectively
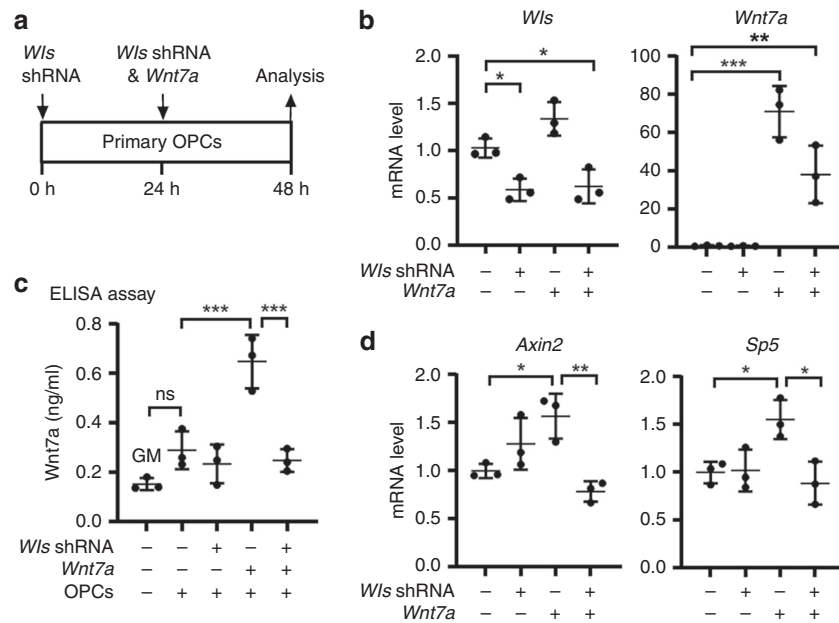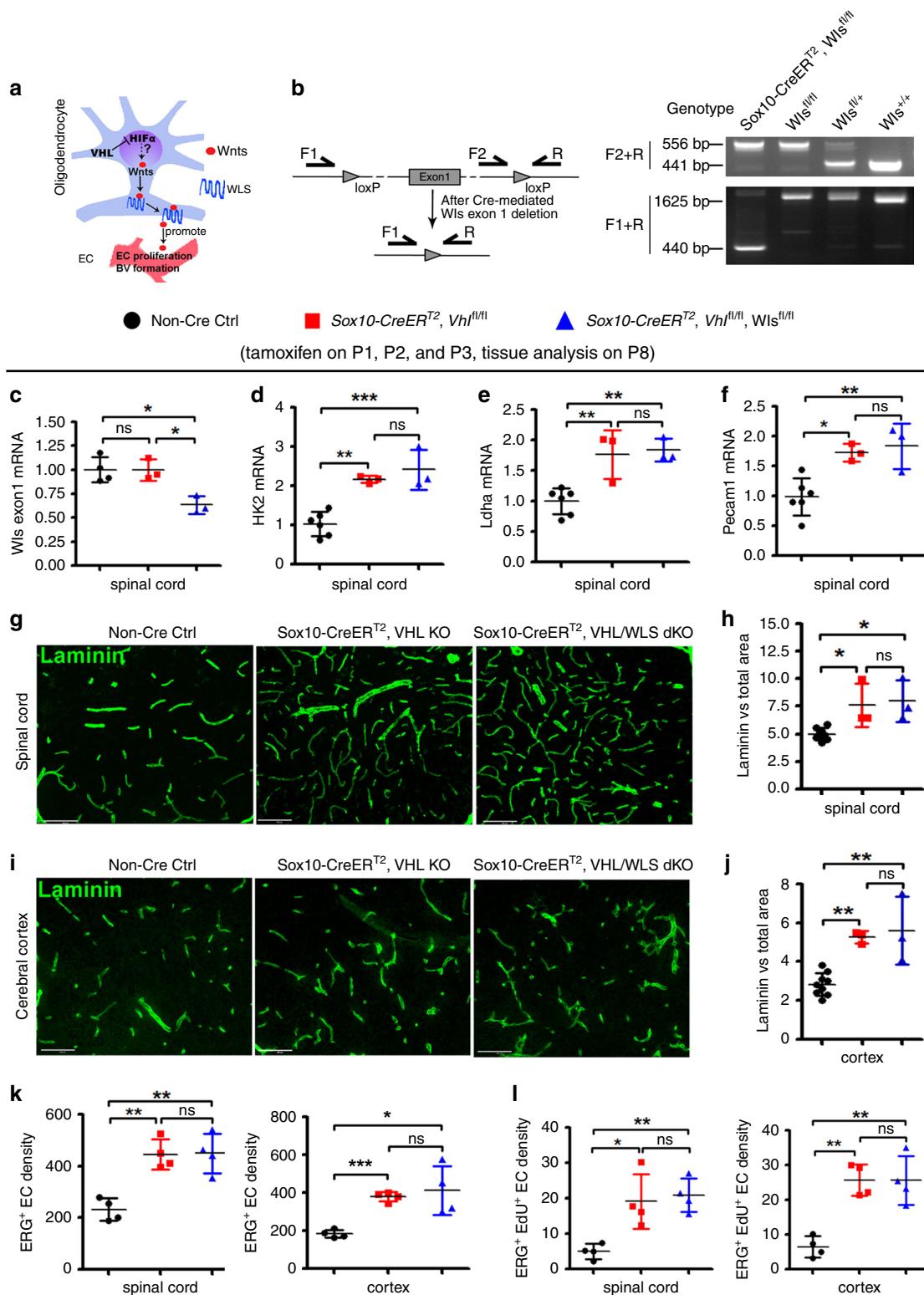
Fig. 3 WLS is required for Wnt secretion from OPCs. a brain primary OPCs growing in the growth medium (GM) were transfected with *Wls*-shRNA and *Wnt7a* plasmids, and OPC mRNA and culture medium were collected for analysis 48 hours (h) after the first *Wls*-shRNA transfection. **b** RT-qPCR assay of *Wls* and *Wnt7a* mRNA in transfected primary OPCs. One-way ANOVA followed by Tukey's multiple comparisons, *$P < 0.05$, **$P < 0.01$, ***$P < 0.001$. $F_{(3,8)}$ = 17.41, $P = 0.007$ *Wls*, $F_{(3,8)}$ = 33.82, $P < 0.0001$ *Wnt7a*. $n = 3$ each group. **c** ELISA measurement of Wnt7a protein concentration in the GM in the absence and presence of OPCs in the dish with Wls-shRNA and Wnt7a transfection. One-way ANOVA followed by Tukey's multiple comparisons, ***$P < 0.001$, ns not significant. $F_{(4,10)} = 21.02$, $P < 0.0001$. Note that Wnt7a concentration in the GM in the presence of primary OPCs is not statistically different from that in the GM in the absence of primary OPCs. $n = 3$ each group. **d** RT-qPCR assay of Wnt target genes *Axin2* and *Sp5* in OPCs. One-way ANOVA followed by Tukey's multiple comparisons, *$P < 0.05$, **$P < 0.01$. $F_{(3,8)}$ = 9.632, $P = 0.0049$ *Axin2*, $F_{(3,8)}$ = 6.965, $P = 0.0128$ *Sp5*. $n = 3$ each group. Data are shown as mean ± s.d. Source data of **b**–**d** are provided as a Source Data file.

suggest that oligodendroglia-derived Wnt signaling is dispensable for HIFα-regulated CNS angiogenesis in vivo.

Oligodendroglial HIFα activates VEGFA. A previous study reported that VEGFA was unperturbed by oligodendroglial HIFα stabilization[9]. We revisited the potential connection between HIFα and VEGFA in oligodendrocytes both in vivo and in vitro. HIF1α cKO (or HIF2α cKO) alone did not alter *Vegfa* mRNA level in the CNS of *Cnp-Cre:Hif1α*^{fl/fl} (or *Cnp-Cre:Hif2α*^{fl/fl}) mutants compared with non-Cre controls (data not shown), indicating a redundancy of oligodendroglial HIF1α and HIF2α in regulating VEGFA. HIFα double cKO (i.e., *Cnp-Cre:Hif1α*^{fl/fl}: *Hif2α*^{fl/fl}) decreased *Vegfa* mRNA expression in the spinal cord (Fig. 6a) and reduced the secretion of VEGFA from primary brain OPCs into the culture medium (Fig. 6b). Conversely, genetic HIFα stabilization by VHL deletion increased *Vegfa* mRNA expression in the spinal cord of *Cnp-Cre:Vhl*^{fl/fl} animals (Fig. 6c, d1–d4). Double fluorescent in situ hybridization confirmed that *Vegfa* mRNA was upregulated in *Plp* mRNA+ oligodendroglial lineage cells in vivo (Fig. 6e1–e2). Moreover, time-conditional and stage-specific VHL cKO demonstrated that genetic HIFα stabilization activated VEGFA not only in PDGFRα+ OPCs (*Pdgfrα-CreER*[T2]*:Vhl*^{fl/fl} strain) (Fig. 6f) but also in PLP+ oligo-dendroglia (*Plp-CreER*[T2]*:Vhl*^{fl/fl} strain) (Fig. 6g). Pharmacological DMOG treatment increased *Vegfa* mRNA expression and HIFα signaling blocker Chetomin prevented DMOG-induced *Vegfa* activation in primary OPCs purified from neonatal murine brains (Fig. 6h). Furthermore, *Vegfa* mRNA was elevated by greater than 3-fold in primary OPCs purified from neonatal *Sox10-Cre:Vhl*^{fl/fl} mice compared with those from non-Cre littermate controls (Fig. 6i). All these data suggest that VEGFA is regulated by HIFα in oligodendroglial lineage cells.

Oligodendroglial HIFα regulates angiogenesis through VEGFA. The regulation of VEGFA by oligodendroglial HIFα led us to hypothesize that VEGFA may be a crucial downstream molecule that couples oligodendroglial HIFα and CNS endothelial cell proliferation and vessel formation. To test this hypothesis, we generated *Pdgfrα-CreER*[T2]*:Vhl*^{fl/fl}*:Vegfa*^{fl/fl} (HIFα-stabilized/ VEGFA-disrupted), *Pdgfrα-CreER*[T2]*:Vhl*^{fl/fl} (HIFα-stabilized), and non-Cre control mice (Fig. 7a, b). The mRNA level of EC-specific marker PECAM1 was significantly attenuated in the spinal cord of *PdgfrαCreER*[T2]*:Vhl*^{fl/fl}*: Vegfa*^{fl/fl} mice compared with that of *Pdgfrα-CreER*[T2]*:Vhl*^{fl/fl} mice (Fig. 7c). The densities of blood vessels (Fig. 7d, e), ERG+ total ECs (Fig. 7f), and ERG +BrdU+ proliferating ECs (Fig. 7g) were all significantly reduced in the spinal cord and cerebral cortex of *Pdgfrα-CreER*[T2]*:Vhl*^{fl/fl}*: Vegfa*^{fl/fl} mice compared with those of *Pdgfrα-CreER*[T2]*:Vhl*^{fl/fl} mice. These data demonstrate that VEGFA disruption attenuates oligodendroglial HIFα-regulated CNS angiogenesis, thus provid-ing unambiguous in vivo data arguing for an essential role of VEGFA in coupling oligodendroglial HIFα function and CNS angiogenesis.

Astroglial HIFα regulates CNS angiogenesis via Wnt signaling. Astroglial maturation is also temporally and functionally coupled with postnatal CNS angiogenesis. We assess the connection of astroglial HIFα and Wnt/β-catenin activation in the CNS. We first used the mouse *Gfap* promoter-driven constitutive Cre, i.e. *mGfap-Cre* to genetically stabilize HIFα in astroglia. The effi-ciency of *mGfap-Cre*-mediated recombination among astroglial lineage cells, quantified by Cre-mediated EYFP reporter, was low (~35%) in the CNS in the early postnatal CNS by P10 (Supple-mentary Fig. 12a–c) and progressively increased during postnatal CNS development (Supplementary Fig. 12d–f). Our fate-mapping

Figure legend key: ● Non-Cre Ctrl　　■ Sox10-CreER^T2, Vhl^fl/fl　　▲ Sox10-CreER^T2, Vhl^fl/fl, Wls^fl/fl

(tamoxifen on P1, P2, and P3, tissue analysis on P8)

data showed that EYFP reporter, which is an indicator of *mGfap-Cre* activity, was expressed in GFAP$^+$ or S100β$^+$ astrocytes, but not in Sox10$^+$ oligodendroglial lineage cells, NeuN$^+$ neurons (Fig. 8a), or ERG$^+$ ECs (data not shown) in the spinal cord and the cerebral cortex of adult *mGfap-Cre:Rosa26-EYFP* mice at P60, confirming that *mGfap-Cre* primarily targets astroglial lineage cells in those CNS regions.

We observed a significant increase in the density of Laminin$^+$ blood vessels (Fig. 8b, c) and in the mRNA expression of EC-specific

PECAM1 (Fig. 8d) throughout the CNS of *mGfap-Cre:Vhl*^fl/fl mutants compared with non-Cre control mice by P30 when Cre-mediated recombination efficiency was greater than 80% (Fig. 8a, Supplementary Fig. 12). Double immunohistochemistry showed that blood-borne macromolecule IgG was confined to Laminin$^+$ blood vessels in *mGfap-Cre:Vhl*^fl/fl mice, a similar pattern to that in age-matched non-Cre controls (Fig. 8e, arrowheads), indicating that the function of the blood-brain (spinal cord) barrier does not appear compromised although the vessel density is elevated.

Fig. 4 Blocking Wnt secretion from oligodendroglial lineage cells does not affect HIFα-regulated CNS angiogenesis. a Schematic diagram depicting putative regulation between HIFα-Wnt axis in glio-vascular units. **b** Primer design (left) and PCR detection (right) of *Wls* gene deletion. Primer pair of F2/R is for detecting *Wls* floxed allele (556bp). After Cre-mediated deletion, primer pair F1/R generates a 410 bp product from the genome of *Sox10-CreER^T2^*, *Wls*^fl/fl^ mice. **c** RT-qPCR assay of exon 1-coding *Wls* mRNA. One-way ANOVA followed by Tukey's multiple comparisons, *$P < 0.05$, ns, not significant. $F_{(2,7)} = 10.39$, $P = 0.008$. $n = 4$ Ctrl, 3 VHL cKO, 3 VHL/WLS cKO. **d–f**, RT-qPCR assay of *Hk2*, *Ldha*, and *Pecam1* mRNA. One-way ANOVA followed by Tukey's multiple comparisons, *$P < 0.05$, **$P < 0.01$, *** $P < 0.001$, ns, not significant. $F_{(2,9)} = 21.73$, $P = 0.0004$ *Hk2*, $F_{(2,9)} = 14.14$, $P = 0.0017$ *Ldha*, $F_{(2,9)} = 10.39$, $P = 0.0046$ *Pecam1*. $n = 6$ Ctrl, 3 VHL cKO, 3 VHL/WLS cKO. **g**, **h** Representative confocal images of Laminin-positive blood vessels in the spinal cord and the percent of Laminin-positive BV area among total assessed area. One-way ANOVA followed by Tukey's multiple comparisons, *$P < 0.05$, ns, not significant. $F_{(2,11)} = 8.8$, $P = 0.0052$. $n = 8$ Ctrl, 3 VHL cKO, 3 VHL/WLS cKO. Scale bars = 100 μm. **i**, **j** Representative confocal images of Laminin-positive blood vessels in the forebrain cerebral cortex and the percent of Laminin-positive BV area among total assessed area. One-way ANOVA followed by Tukey's multiple comparisons, **$P < 0.01$, ns, not significant. $F_{(2,12)} = 16.47$, $P = 0.0004$. $n = 9$ Ctrl, 3 VHL cKO, 3 VHL/WLS cKO. Scale bars = 100 μm. **k** Densities (#/mm^2) of ERG$^+$ endothelial cells. One-way ANOVA followed by Tukey's multiple comparisons, *$P < 0.05$, **$P < 0.01$, ns, not significant. $F_{(2,9)} = 16.89$, $P = 0.0009$ spinal cord; Welch's ANOVA followed by unpaired t test with Welch's correction, $W_{(2,5.346)} = 65.98$, $P = 0.0002$ cortex. $n = 4$ Ctrl, 4 VHL cKO, 4 VHL/WLS cKO. **l** Densities (#/mm^2) of ERG$^+$/EdU$^+$ proliferating endothelial cells (2 h EdU pulse labeling prior to tissue harvesting at P8). One-way ANOVA followed by Tukey's multiple comparisons, *$P < 0.05$, **$P < 0.01$, ns, not significant. $F_{(2,9)} = 10.63$, $P = 0.0043$ spinal cord, $F_{(2,9)} = 18.43$, $P = 0.0007$ cortex. $n = 4$ Ctrl, 4 VHL cKO, 4 VHL/WLS cKO. Data are shown as mean ± s.d. Source data of **c–f**, **h**, **j**, **k**, **l** are provided as a Source Data file.

Unexpectedly, we found that stabilizing HIFα in astroglial lineage cells (Fig. 8f) remarkably activated Wnt/β-catenin signaling in the CNS of *mGfap-Cre:Vhl*^fl/fl^ mice, as shown by significant elevation in the expression of Wnt/β-catenin signaling target genes *Axin2* and *Notum* in spinal cord and brain (Fig. 8g). Histological (Fig. 8h) and Western blot (cf Fig. 9a, b) assay demonstrated that the active form of β-catenin (dephosphorylated on Ser37 or Thr41) was significantly increased in *mGfap-Cre:Vhl*^fl/fl^ mice. Double immunohistochemistry confirmed the presence of elevated active β-catenin in PECAM1$^+$ ECs (Fig. 8i, arrowheads). Collectively, our data suggest that stabilizing HIFα in astroglial lineage cells increases CNS angiogenesis and activates Wnt/β-catenin signaling in ECs.

Wnt/β-catenin signaling activation in ECs by astroglial HIFα stabilization led us to hypothesize that astroglia-derived Wnt signaling may instead play a major role in HIFα-regulated CNS angiogenesis. To test this hypothesis, we generated *mGfap-Cre:Vhl*^fl/fl^:*Wls*^fl/fl^ mice to stabilize HIFα's function and simultaneously disrupting Wnt secretion from HIFα-stabilized astroglia. Our data showed that Wnt signaling activity was significantly reduced in the spinal cord of *mGfap-Cre:Vhl*^fl/fl^:*Wls*^fl/fl^ mice compared with that of *mGfap-Cre:Vhl*^fl/fl^ mice (Fig. 9a, b), thus verifying the efficacy of blocking astroglia-derived Wnt signaling in vivo by WLS deletion. Intriguingly, disrupting astroglia-derived Wnt signaling significantly reduced the densities of blood vessels (Fig. 9c–e) and ERG$^+$ ECs (Fig. 9f–h) in the CNS of *mGfap-Cre:Vhl*^fl/fl^:*Wls*^fl/fl^ double mutant mice compared with *mGfap-Cre:Vhl*^fl/fl^ mice, indicating that astroglia-derived Wnt signaling is a downstream mediator of astroglial HIFα-regulated CNS angiogenesis.

Our results indicated that the constitutive mGfap-Cre elicited a poor recombination efficiency in early postnatal astrocytes (Supplementary Fig. 12). To determine whether early postnatal astrocytes regulate CNS angiogenesis through HIFα-activated Wnt signaling, we generated *Aldh1l1-CreER^T2^:Vhl*^fl/fl^:*Wls*^fl/fl^ mutants. Our data demonstrated a greater than 90% of recombination efficiency and 95% of astroglial specificity in the spinal cord and cerebral cortex of *Aldh1l1-CreER^T2^:Rosa26-EYFP* at P8 when tamoxifen was injected at P1, P2 and P3 (Supplementary Fig. 13). Consistent with the data derived from *mGfap-Cre:Vhl*^fl/fl^:*Wls*^fl/fl^ strain, we found that the densities of blood vessels and ECs were significantly increased in *Aldh1l1-CreER^T2^:Vhl*^fl/fl^ mutants compared with those in non-Cre controls and that simultaneous WLS ablation significantly reduced the densities of blood vessels and ECs in the cortex and spinal cord of *Aldh1l1-CreER^T2^:Vhl*^fl/fl^:*Wls*^fl/fl^ mutants

compared with those of *Aldh1l1-CreER^T2^:Vhl*^fl/fl^ animals at early postnatal age of P8 (Fig. 10). These data provide a strong genetic proof that HIFα-activated Wnt signaling is a major downstream pathway by which astroglia regulate angiogenesis during postnatal CNS development.

Discussion

The maturation of glial cells including oligodendroglia and astroglia in the developing human and murine brain is temporally and functionally coupled with the maturation of the CNS vascular network[21]. The regulation of CNS angiogenesis by glial cells is critical for postnatal CNS development and investigating the molecular underpinnings of CNS angiogenesis has clinical implications in neural repair after CNS damage in which hypoxia is commonly present[4,21,22]. In this study, we employed a battery of genetic mutant mice and presented several significant findings: (1) oligodendroglial HIFα is necessary and sufficient for postnatal CNS angiogenesis and this regulation occurs in a manner independent of CNS regions; (2) in sharp contrast to the previous report[9], HIFα stabilization in oligodendroglial lineage cells does not perturb Wnt/β-catenin signaling, but remarkably activates VEGF, and genetically blocking oligodendroglia-derived VEGF but not Wnt reduces oligodendroglial HIFα-regulated CNS angiogenesis; (3) Wnt signaling is a downstream pathway by which astroglial HIFα regulates CNS angiogenesis. Our findings represent an alternative view in our mechanistic understanding of oligodendroglial HIFα-regulated angiogenesis from a Wnt-dependent/VEGF-independent view[9] to a VEGF-dependent/Wnt-independent one, and also unveil a glial cell type-dependent HIFα-Wnt axis (oligodendroglial vs astroglia) in regulating CNS angiogenesis (Supplementary Fig. 14).

Previous data suggested that the regulation of Wnt/β-catenin signaling (activation or repression) by HIFα is cell type and/or context-dependent[10,23–27]. It is important to determine whether HIFα in CNS glial cells differentially regulates Wnt/β-catenin signaling in vivo. A recent study reported that oligodendroglial HIFα could activate Wnt/β-catenin signaling not only in oligodendroglial lineage cells but also in endothelial cells through HIFα-mediated Wnt7a/7b expression[9]. However, the in vivo and in vitro data presented in this study do not support this assertion. Here, we employed five different strains of oligodendroglial Cre (two constitutive Cre and three inducible Cre) to genetically stabilize HIFα and found no evidence of Wnt/β-catenin activation or Wnt7a/7b upregulation in the brain and the spinal cord and in primary OPCs. The failure to detect Wnt/β-catenin activation is unlikely due to the inefficiency of HIFα stabilization because the
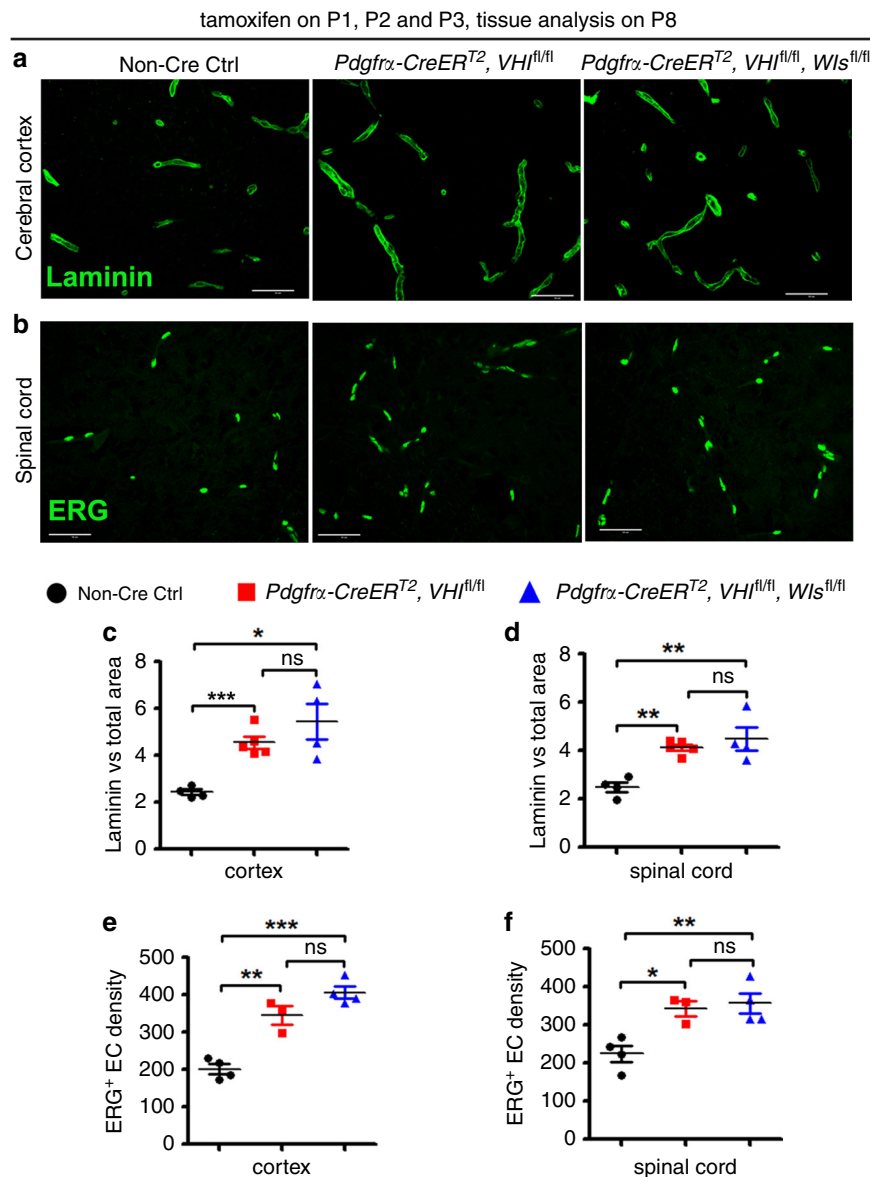
Fig. 5 Blocking Wnt secretion from oligodendrocyte progenitor cells (OPCs) does not affect HIFα-regulated CNS angiogenesis. a, b Representative confocal images of Laminin-labeled blood vessels and ERG-labeled ECs in each group of mice. Scale bars = 50 μm. **c, d** Percent of Laminin-occupying area among total assessed area. Welch's ANOVA followed by unpaired t test with Welch's correction, *$P < 0.05$, ***$P < 0.001$, ns, not significant. $W_{(2,5.256)} = 30.38$, $P = 0.0013$ for cortex. One-way ANOVA followed by Tukey's multiple comparisons, **$P < 0.01$, ns, not significant. $F_{(2,10)} = 12.67$, $P = 0.0018$ for spinal cord. $n = 4$ Ctrl, 5 VHL cKO, 4 VHL/WLS cKO. **e, f** Densities (#/mm^2) of ERG$^+$ ECs. One-way ANOVA followed by Tukey's multiple comparisons, *$P < 0.05$, **$P < 0.01$, ***$P < 0.001$, ns, not significant. $F_{(2,8)} = 39.80$, $P < 0.0001$ cortex, $F_{(2,8)} = 10.30$, $P = 0.0064$ spinal cord. Mice from the above three groups were injected with tamoxifen at P1, P2, and P3 and sacrificed at P8. $n = 4$ Ctrl, 3 VHL cKO, 4 VHL/WLS cKO. Data are shown as mean ± s.d. Source data of **c–f** are provided as a Source Data file.

canonical HIFα target genes, for example, those which are involved in glycolysis, are consistently and significantly upregulated in our transgenic animals and in primary OPCs, thus verifying the efficacy of HIFα stabilization. In sharp contrast, we found that Wnt/β-catenin signaling activity is significantly upregulated in the CNS of astroglial HIFα-stabilized mice, suggesting that our experimental approach is effective in quantifying the changes of Wnt/β-catenin activity and that the regulation of Wnt/β-catenin signaling by HIFα is glial cell type-dependent in the CNS.

Inspired by glial cell type (oligodendroglia vs astroglia)-dependent activation of Wnt/β-catenin signaling, we proposed a working model in which HIFα-activated Wnt signaling regulates endothelial cell proliferation and vessel formation in a

cell type-dependent manner (Supplementary Fig. 14). To avoid the intrinsic caveats of pharmacological compounds and in vitro culture systems, we employed in vivo genetic models of VHL/WLS double cKO to stabilize HIFα and simultaneously disrupt the secretion of Wnt ligands. Indeed, our data demonstrate that WLS-deficiency decreases Wnt secretion and Wnt7a-induced autocrine Wnt/β-catenin signaling in primary OPCs and that disrupting WLS in astroglia reduces the activity of astroglial HIFα-regulated Wnt/β-catenin signaling in the CNS. Based on VHL/WLS double cKO systems, we provide strong genetic evidence that HIFα-regulated Wnt signaling from astroglia but not oligodendroglia plays a crucial role in regulating postnatal CNS angiogenesis. Our findings argue against a major role oligodendroglia-derived/HIFα-activated
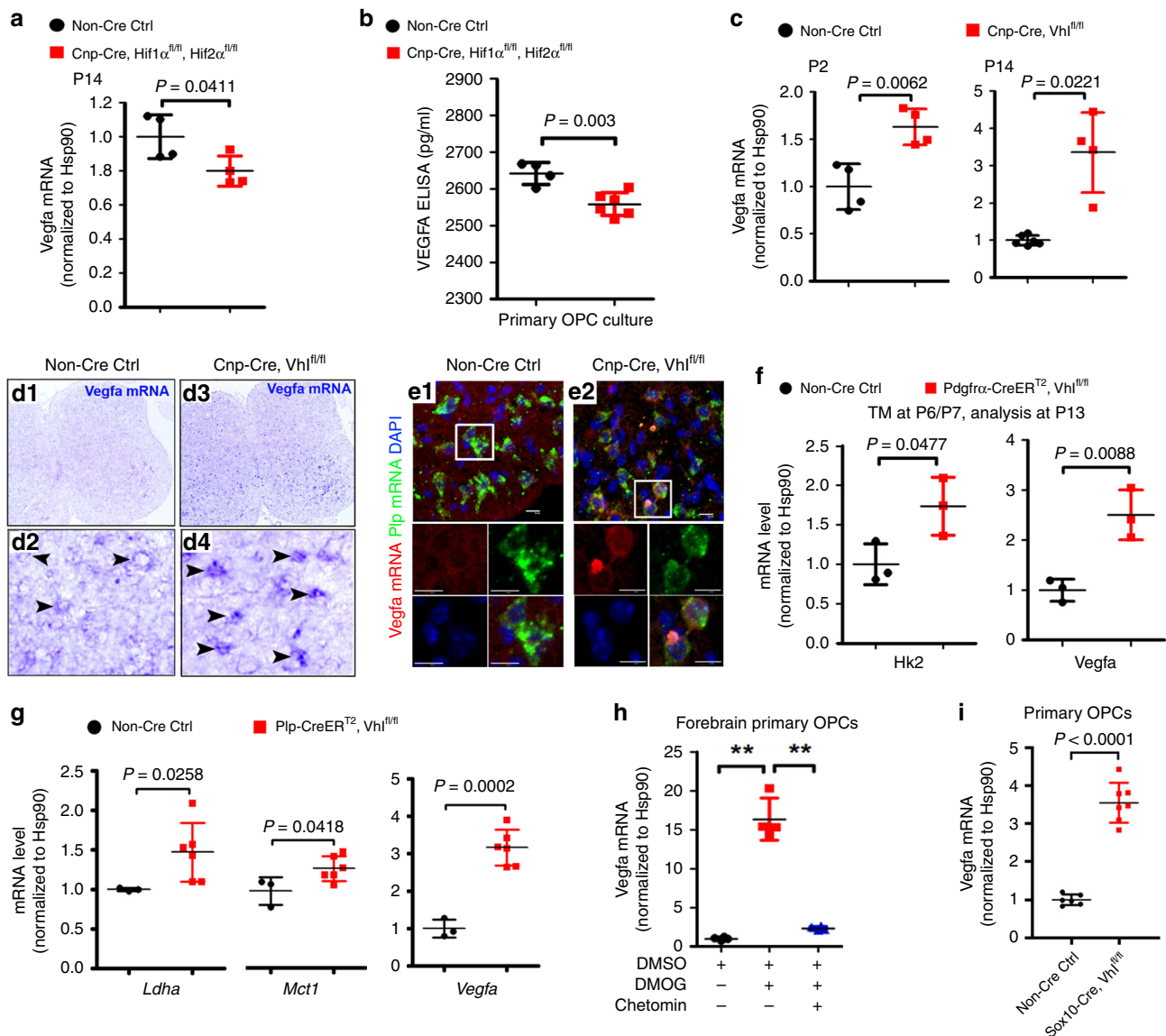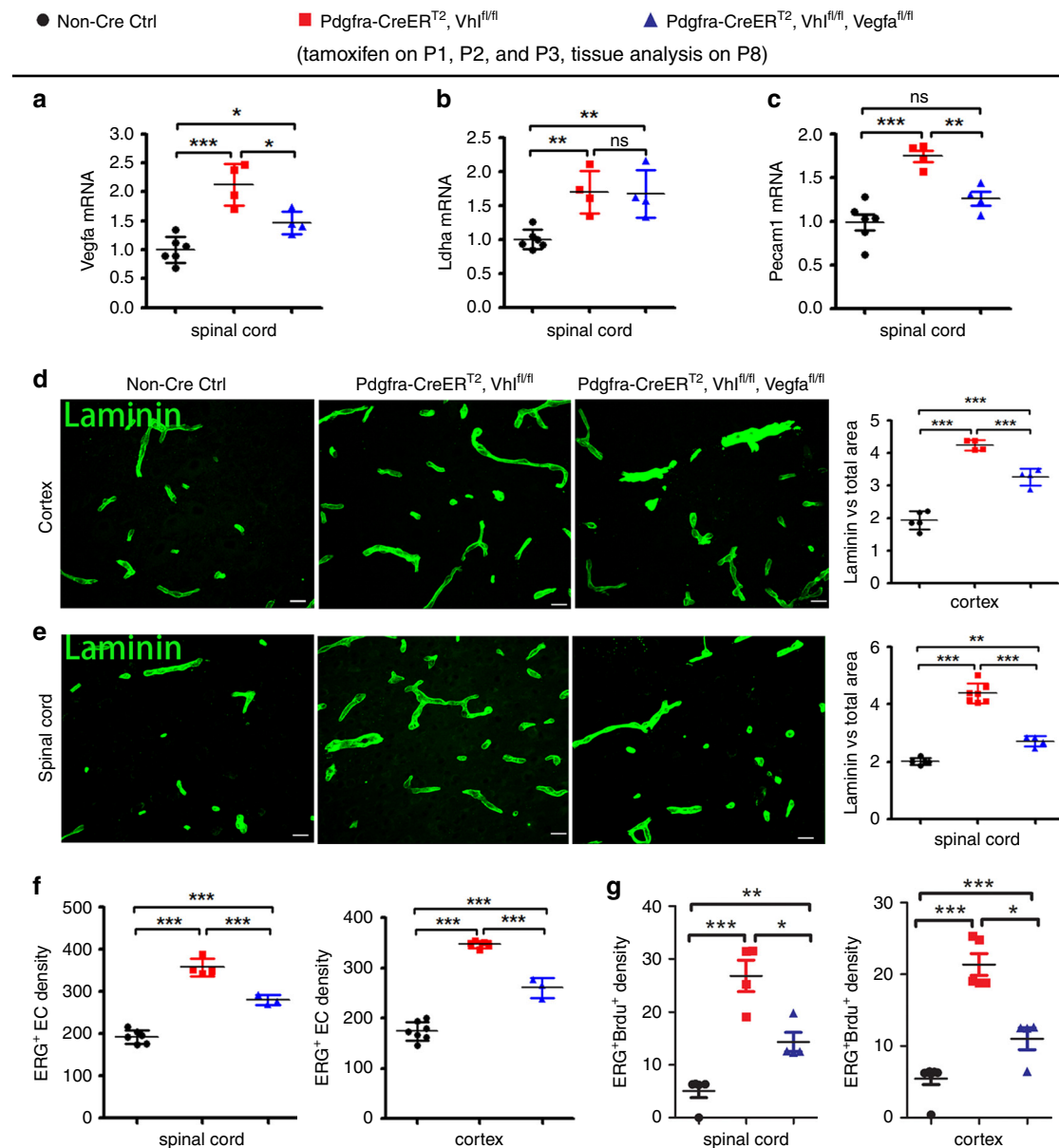
Fig. 6 Oligodendroglial HIFα regulates VEGFA expression. a RT-qPCR assay of *Vegfa* mRNA in the spinal cord of P14 mice. Two-tailed Student's *t* test, $t_{(6)} = 2.590$. $n = 4$ Ctrl, 4 HIFα cKO. **b** ELISA measurement of VEGFA concentration in the culture medium of primary OPCs isolated from neonatal forebrain of indicated genotypes. Two-tailed Student's *t* test, $t_{(8)} = 4.208$. $n = 4$ Ctrl, 6 HIFα cKO. **c** RT-qPCR assay of *Vegfa* mRNA in the spinal cord. Two-tailed Student's *t* test, $t_{(6)} = 4.127$ at P2; Welch's correction $t_{(3.139)} = 4.299$ at P14. $n = 4$ each group. **d1–d4** *Vegfa* mRNA in situ hybridization in the spinal cord of P8 transgenic mice. Arrowheads point to *Vegfa* mRNA+ cells. Note that *Vegfa* mRNA signals were higher in the *Cnp-Cre, Vhl*fl/fl spinal cord (**d2**) than those in the non-Cre controls (**d4**). **e1–e2** *Vegfa* and *Plp* dual fluorescent mRNA in situ hybridization in P8 spinal cord. Boxed areas were shown at higher magnification in single color channels. Note that *Vegfa* mRNA signals are higher in *Plp*+ oligodendrocytes in *Cnp-Cre, Vhl*fl/fl mutants than those in non-Cre controls. Scale bars: 10 μm. **f** RT-qPCR assay of *Hk2* and *Vegfa* mRNA in the spinal cord of P14 *Pdgfrα-CreER*T2*, Vhl*fl/fl and non-Cre littermate controls that had been treated with tamoxifen (TM) at P6 and P7. Two-tailed Student's *t* test, $t_{(4)} = 2.822$ *Hk2*, $t_{(4)} = 4.770$ *Vegfa*. $n = 3$ each group. **g** RT-qPCR assay of the mRNA levels of HIFα target genes *Ldha, and Mct1* and *Vegfa* in the spinal cord of P14 *Plp-CreER*T2*, Vhl*fl/fl and non-Cre littermate controls that had been treated with tamoxifen at P6 and P7. Two-tailed Student's *t* test, $t_{(7)} = 2.487$ *Mct1*, $t_{(7)} = 7.194$ *Vegfa*; Two-tailed Student's *t* test with Welch's correction, $t_{(5.079)} = 3.116$ *Ldha*. **h** RT-qPCR assay of *Vegfa* mRNA in primary OPCs treated with HIFα stabilizer MOG and inhibitor Chetomin (cf Supplementary Fig. 9). Welch's ANOVA followed by unpaired *t* test with Welch's correction, **$P < 0.01$. $W_{(2,5.270)} = 79.93$, $P = 0.0012$. $n = 4$ each group. **i** RT-qPCR assay of *Vegfa* mRNA in primary OPCs isolated from neonatal brains of Sox10-Cre, *Vhl*fl/fl mutants and littermate controls. Two-tailed Student's *t* test, Welch's-corrected $t_{(7.008)} = 12.38$. $n = 3$ Ctrl, 7 VHL cKO. Data are shown as mean ± s.d. Source data of **a–c**, **f–i** are provided as a Source Data file.

Wnt/β-catenin signaling in angiogenesis in the developing murine CNS as previously reported[9].

There are 19 Wnt ligands in rodents, which can be grossly classified into canonical and non-canonical sub-types depending on the necessity of β-catenin for the signaling activation[10]. WLS ablation blocks the secretion of all Wnt members from Wnt-producing cells[16–19,28]. In our genetic models, we demonstrate that ablation of WLS remarkably reduces astroglial

HIFα-mediated canonical Wnt/β-catenin signaling. However, we cannot exclude the possibility that astroglia-derived non-canonical Wnt signaling is also altered in our genetic manipulation which may be potentially involved in CNS angiogenic regulation[29]. Moreover, it remains unclear which Wnt ligand(s) plays a major role in coupling astroglial HIFα with CNS angiogenesis. Our preliminary data do not support a major role of Wnt7a/7b, because neither Wnt7a nor Wnt7b expression was

Fig. 7 Oligodendroglial HIFα regulates CNS angiogenesis through VEGFA-mediated signaling. a–c RT-qPCR assay of the mRNA levels of *Vegfa, Ldha,* and *Pecam1* in the spinal cord of each group of mice. One-way ANOVA followed by Tukey's multiple comparisons, $*P < 0.05$, $**P < 0.01$, $***P < 0.001$, ns not significant. $F_{(2,11)} = 21.74$, $P = 0.0002$ *Vegfa*; $F_{(2,11)} = 11.50$, $P = 0.0020$ *Ldha*; $F_{(2,11)} = 20.31$, $P = 0.0002$ *Pecam1*. n = 6 Ctrl, 4 VHL cKO, 4 VHL/VEGFA cKO. **d, e** Representative confocal images and quantification of Laminin-positive blood vessels. One-way ANOVA followed by Tukey's multiple comparisons, $**P < 0.01$, $***P < 0.001$, ns not significant. $F_{(2,10)} = 105.5$, $P < 0.0001$ cortex, $n = 5$ Ctrl, 4 VHL cKO, 4 VHL/VEGFA cKO.; $F_{(2,13)} = 133.2$, $P < 0.0001$ spinal cord, n = 5 Ctrl, 7 VHL cKO, 4 VHL/VEGFA cKO. Scale bars = 10 μm. **f, g** densities (#/mm²) of ERG⁺ ECs and ERG⁺BrdU⁺ proliferating ECs. One-way ANOVA followed by Tukey's multiple comparisons, $*P < 0.05$, $**P < 0.01$, $***P < 0.001$. ERG⁺ ECs, $F_{(2,10)} = 113.1$, $P < 0.0001$ spinal cord, $n = 6$ Ctrl, 4 VHL cKO, 3 VHL/VEGFA cKO; $F_{(2,12)} = 169.0$, $P < 0.0001$ cortex, $n = 7$ Ctrl, 5 VHL cKO, 3 VHL/VEGFA cKO; ERG⁺BrdU⁺ proliferating ECs, $F_{(2,10)} = 24.09$, $P = 0.0001$ spinal cord, $n = 5$ Ctrl, 4 VHL cKO, 4 VHL/VEGFA cKO; $F_{(2,12)} = 86.14$, $P < 0.0001$ cortex, $n = 7$ Ctrl, 5 VHL cKO, 4 VHL/VEGFA cKO. Data are shown as mean ± s.d. Source data of **a–g** are provided as a Source Data file.

activated in oligodendroglial and astroglial HIFα-stabilized CNS. Future studies are needed to pinpoint which Wnt ligand (s) are the downstream mediator(s) of astroglial HIFα-regulated CNS angiogenesis.

VEGF (i.e. VEGFA) is a well-established angiogenic and neurotrophic factor in the CNS[4,30–35]. VEGFA regulates angiogenesis in the developing and adult CNS through its membrane-bound receptors VEGFR-1(Flt1) and VEGFR-2 (Kdr)[30]. In the early postnatal CNS, VEGFR-1 and 2 are highly expressed in the vascular ECs. However, the ligand VEGFA is barely detectable in the vascular ECs but highly expressed in the parenchymal neural cells

including oligodendroglial lineage cells[20,36–38]. The previous study suggested that the HIFα-VEGF connection did not occur in the CNS oligodendroglia[9] although this connection was demonstrated in the retina[39]. In this study, we found that oligodendroglial HIFα cKO reduces VEGFA whereas oligodendroglial HIFα stabilization increases VEGFA expression, indicating that HIFα transcriptionally regulates VEGFA in oligodendroglial lineage cells. Further corroborating these findings, purified primary OPCs respond to HIFα signaling stabilizer (DMOG) and blocker (Chetomin) by activating and inactivating VEGFA, respectively. Our results are consistent with previous data showing
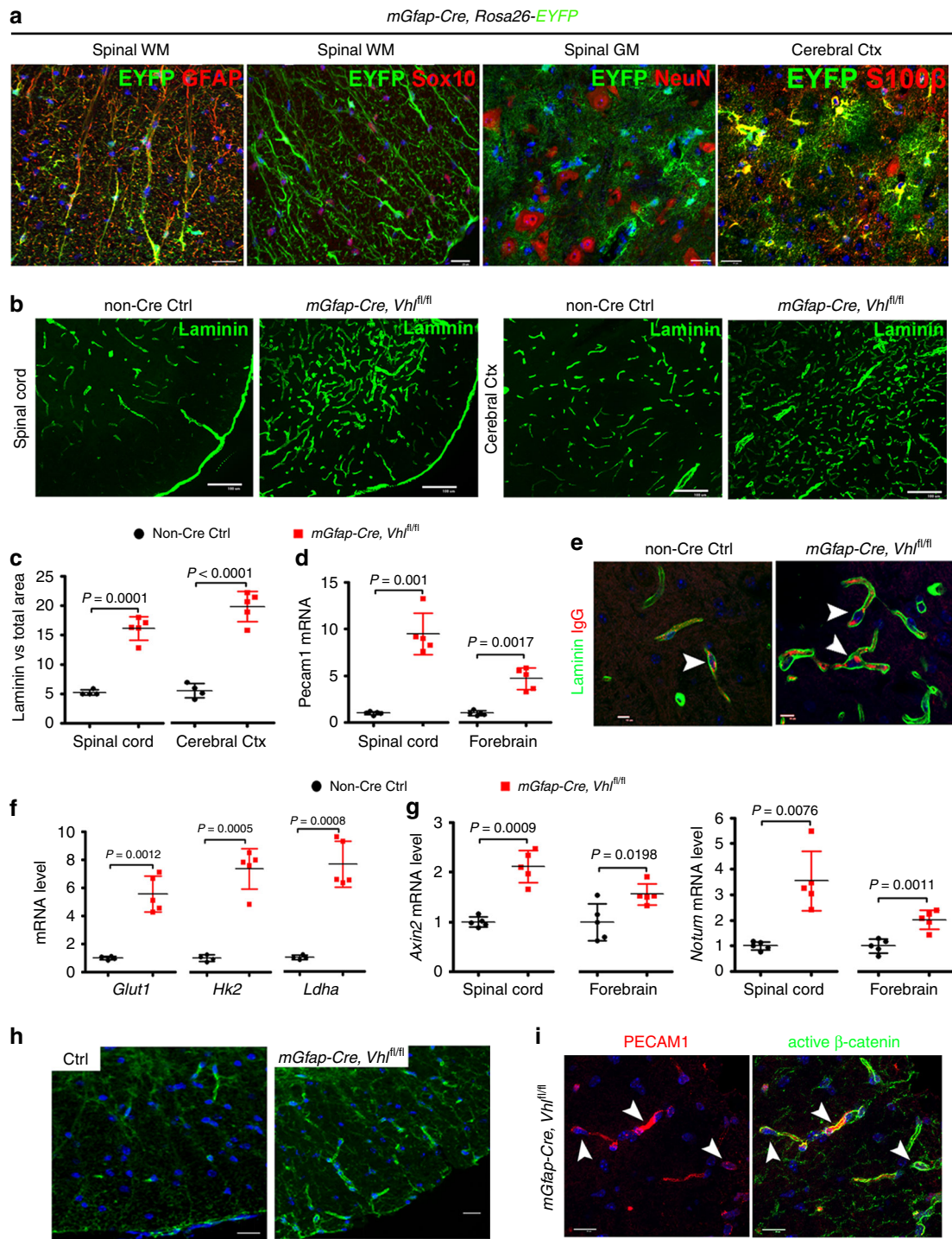
that VEGFA is a direct transcriptional target of HIFα[40–42]. By leveraging our unique in vivo genetic models of VHL/VEGFA double cKO, we unequivocally prove that VEGFA is an essential downstream molecule that couples oligodendroglial HIFα function and vascular angiogenesis in the CNS, which is different from Yuen et al.[9], who reported that VEGFA was unchanged in the CNS of oligodendroglial HIFα-stabilized mutants. The discrepancy may presumably reflect the intrinsic differences of in vitro pharmacological interventions and in vivo genetic manipulations.

It has been suggested that Wnt signaling regulates VEGF, or vice versa, to control angiogenesis[43–45]. It is possible that Wnt/β-catenin signaling is required for, or synergistically regulates, HIFα-activated VEGFA expression. Our data do not support this possibility. First, stabilizing oligodendroglial HIFα activates VEGFA but not Wnt/β-catenin signaling. Second, VEGF expression is indistinguishable in the CNS of oligodendroglial VHL/WLS double cKO mutants from that of oligodendroglial VHL single cKO mutants (data not shown), indicating that oligodendroglial-derived Wnt signaling plays a minor role in VEGFA expression. Third, Wnt/β-catenin activity is comparable in the CNS of oligodendroglial VHL/VEGFA double cKO mutants and VHL single cKO mutants, implying that oligodendroglia-derived VEGFA has no regulatory role in

Fig. 8 Astroglial HIFα stabilization promotes CNS angiogenesis and enhances Wnt signaling activity. a Fate-mapping study showing that mGfap-Cre-mediated EYFP was expressed in GFAP+ astrocytes but not in Sox10+ oligodendroglial lineage cells or NeuN+ neurons in the spinal cord at P60. WM, white matter, GM, gray matter, Ctx, cortex. EYFP was identified as S100β+ astrocytes in the cerebral Ctx. Scale bars = 20 μm. **b** Representative images of Laminin immunostaining in *mGfap-Cre, Vhl*fl/fl mutants and non-Cre control mice at P30. Scale bars = 100 μm. **c** Percentage of Laminin-occupying area among total area at P30. Two-tailed Student's *t* test, Welch's corrected $t_{(4)} = 11.92$ spinal crd, $t_{(7)} = 10.12$ cerebral cortex. $n = 4$ Ctrl, 5 VHL cKO. **d** RT-qPCR assay of endothelial Pecam1 at P30. Two-tailed Student's *t* test, Welch's corrected $t_{(4.046)} = 8.564$ spinal cord, Welch's corrected $t_{(4.490)} = 6.706$ forebrain. $n = 5$ each group. **e** immunostaining showing that endogenous mouse IgG is restricted to Laminin+ blood vessels (arrowheads) in the early adult spinal cord of *mGfap-Cre,Vhl*fl/fl mutant and control mice at P47. Scale bars = 10 μm. **f** RT-qPCR assay of the mRNA levels of HIFα target gene *Glut1, Hk2* and *Ldha* in P30 spinal cord. Two-tailed Student's *t* test with Welch's correction, $t_{(4.099)} = 7.947$ *Glut1*, $t_{(4.243)} = 9.636$ *Hk2*, $t_{(4.085)} = 9.025$ *Ldha*. $n = 4$ Ctrl, 5 VHL cKO. **g** RT-qPCR assay of the mRNA levels of Wnt/β-catenin target genes *Axin2* and *Notum* at P30. Two-tailed Student's *t* test, Welch's corrected $t_{(4.760)} = 7.296$ spinal cord *Axin2*, $t_{(8)} = 2.902$ forebrain *Axin2*, Welch's corrected $t_{(4.149)} = 4.850$ spinal cord *Notum*, $t_{(8)} = 4.994$ forebrain *Notum*. $n = 5$ each group. **h** Immunostaining of active β-catenin in the spinal cord of mGfap-Cre, Vhl fl/fl mutants and non-Cre control mice at P30. Scale bars = 10 μm. **i** Double immunostaining of active β-catenin and PECAM1 in the spinal cord of *mGfap-Cre, Vhl*fl/fl mutants at P30. Arrowheads point to double-positive cells. Blue is DAPI nuclear staining. Scale bars = 10 μm. Data are shown as mean ± s.d. Source data of **c, d, f, g** are provided as a Source Data file.

Wnt/β-catenin activity. Together, our results do not support a major interplay between oligodendroglial HIFα-activated VEGFA and Wnt/β-catenin signaling in modulating CNS angiogenesis.

Previous studies including those from our own laboratory[10,12,46–49] have shown that dysregulated Wnt/β-catenin activity invariably inhibits oligodendrocyte differentiation and myelination. Given the normal level of Wnt/β-catenin activity in the CNS of oligodendroglial HIFα-stabilized mutants, our study will spark renewed interests in studying Wnt-independent mechanisms underlying the impairment of oligodendroglial differentiation and myelination in HIFα-stabilized mutants as previously reported[9]. Interestingly, HIFα is stabilized and enriched in oligodendroglia in the active demyelinating lesions and normal-appearing white matter (NAWM) of multiple sclerosis patient brains[50–53]. We show that HIFα stabilization in oligodendrocytes remarkably activates the angiogenic and neurotrophic factor VEGF in the CNS. The genetic models generated in our study also provide a powerful tool in determining the role of HIFα stabilization in OPCs and oligodendrocytes in the pathophysiology of demyelination and remyelination in multiple sclerosis and other neurological disorders in which hypoxia-like tissue injury occurs.

Methods

Animals. A total of 14 transgenic strains were used in this study. Cnp-Cre mice (RRID: MGI_3051754)[11], Sox10-Cre (RRID: IMSR_JAX:025807), Sox10-CreERT2 (RRID:IMSR_JAX: 027651), Pdgfrα-CreERT2 (RRID: IMSR_JAX:018280), Aldh1l1-CreERT2 (RRID: IMSR_JAX:029655), Plp-CreERT2 (RRID: IMSR_JAX:005975), mGfap-Cre (RRID: IMSR_JAX:024098), Hif1α-floxed (RRID: IMSR_JAX:007561), Hif2α-floxed (RRID: IMSR_JAX:008407), Vhl-floxed (RRID: IMSR_JAX:012933), Wls-floxed (RRID: IMSR_JAX:012888), Vegfa-floxed (MGI:1931048)[54], Bat-lacZ (RRID: IMSR_JAX:005317), Rosa26-EYFP (RRID: IMSR_JAX:006148). Animals were housed at 12h light/dark cycle with free access to food and drink, and both males and females were used in this study. The single transgenic mice were crossed to generate double or triple transgenic mice indicated in the study. All Cre transgene was maintained as heterozygous. All transgenic mice were maintained on a C57BL/6 background. Animal protocols were approved by Institutional Animal Care and Use Committee at the University of California, Davis.

Primers used for genotyping *Hif1α*-floxed, *Hif2α*-floxed, and *Vhl*-floxed and for detecting Cre-mediated DNA deletion (as in Figs. 1a and 2a, b) were derived from previous study[55] and listed here. *Hif1α*-F1: 5′-TTGGGGATGAAAACATCTGC-3′, *Hif1α*-F2: 5′-GCAGTTAAGAGCACTAGTTG-3′, *Hif1α*-R: 5′-GGAGCTATCTC TCTAGACC-3′), *Hif2α*-F1:5′-CAGGCAGTATGCCTGGCTAATTCCAGTT-3′, *Hif2α*-F2: 5′-CTTCTTCCATCATCTGGGATCTGGGACT-3′, *Hif2α*-R: 5′-GCT AACACTGTACTGTCTGAAAGAGTAGC-3′, *Vhl*-F1: 5′-CTGGTACCCACG AAACTGTC-3′, *Vhl*-F2: 5′-CTAGGCACCGAGCTTAGAGGTTTGCG-3′ *Vhl*-R: 5′-CTGACTTCCACTGATGCTTGTCACAG-3′. Primers used for genotyping Wls-floxed for detecting Cre-mediated DNA deletion (as in Fig. 7b) were derived from previous study[18] and listed here. *Wls*-F1: 5′-CTTCCCTGCTTCTTTAAGC GTC-3′, *Wls*-F2: 5′-AGGCTTCGAACGTAACTGACC-3′, *Wls*-R: 5′-CTCAGAAC TCCCTTCTTGAAGC-3′

Tamoxifen and BrdU (or EdU) treatment. Tamoxifen (TM) (T5648, Sigma) was dissolved in mixture of ethanol and sunflower oil (1:9 by volume) at a concentration of 30 mg/ml[14]. Mice were administrated intraperitoneally (i.p.) with tamoxifen at dose of 200 μg/g body weight at time points indicated in each figure. BrdU (B5002, Sigma) or EdU (A10044, Thermo Fisher Scientific) was freshly dissolved in 0.9% sterile saline at a concentration of 10 mg/ml. BrdU or EdU was i. p. injected to animals at a dose of 100 μg/g body weight at time-points indicated in the figures. Tamoxifen was administered to both the controls and the inducible floxed mice in all experiments involving inducible Cre-LoxP approach.

Primary OPC culture. Primary mixed glial culture (MG) was prepared from the forebrains of neonatal pups between ages P0 and P2. The isolated cortical tissues were dissociated by papain dissociation kit (#LK003176, Worthington) supplemented with DNase I (250 U/ml; #D5025, Sigma) and D-(+)-glucose (0.36%; #0188 AMRESCO) in 33 °C/10% CO₂ for 90 min. Next, the tissues were transferred in PDS Kit-Inhibitor solution (#LK003182, Worthington). Tissue chunks were triturated, and then collect the cell suspension supernatant. After centrifugation, cells were plated on poly-D-lysine (PDL, #A003-E, Millipore)-coated 10 cm dishes (#130182, Thermo Scientific) in high-glucose DMEM medium (#1196092, Thermo Fisher) with 10% heat-inactivated fetal bovine serum (#12306-C, Sigma) and penicillin/streptomycin (P/S, #15140122, Thermo Fisher). After 24 h, attached cells were washed with HBSS (#24020117, Thermo Fisher) to remove serum, and maintained with serum-free growth medium (GM), a 3:7 mixture (v/v) of B104 neuroblastoma-conditioned medium, 10 ng/ml Biotin (#B4639, Sigma), and N1 medium (high-glucose DMEM supplemented with 5 μg/ml insulin (#I6634, Sigma), 50 μg/ml apo-transferrin (#T2036, Sigma), 100 μM Putrescine (#P5780, Sigma), 30 nM Sodium selenite (#S5261, Sigma), 20 nM Progesterone (#P0130, Sigma). We performed immunopanning 96 h after GM maintenance. Before immunopanning, cells were resuspended in panning solution (0.1% BSA in N1 medium). The cells were panned once with the anti-Thy1.2 antibody (#105302, Biolegend) for negative immunopanning and then panned once with the anti-NG2 antibody (#AB5320, Millipore) for positive immunopanning. OPCs were cultured on PDL-coated plates with complete GM. The complete GM consisted of GM with 5 ng/ml FGF (#450-33, Peprotech), 4 ng/ml PDGF-AA (#315-17, Peprotech), 50 μM Forskolin (#6652995, Peprotech,) and glutamax (#35050, Thermo Fisher). To induce differentiation, the medium was switched to differentiation medium (DM), which consists of 12.5 μg/ml insulin, 100 μM Putrescine, 24 nM Sodium selenite, 10 nM Progesterone, 10 ng/ml Biotin, 50 μg/ml Transferrin (#T8158, Sigma), 30 ng/ml 3,3′,5-Triiodo-L-thyronine (#T5516, Sigma), 40 ng/ml L-Thyroxine (#T0397, Sigma-Aldrich), glutamax and P/S in F12/high-glucose DMEM, 1:1 in medium (#11330032, Thermo Fisher Scientific).

HIFα signaling stabilization and inhibition in vitro. Purified brain primary OPCs were pre-incubated with 100 nM Chetomin or DMSO control for 2 h, and then switched to the fresh culture medium with 1 mM Dimethyloxalylglycine (DMOG, D3695, Sigma) in the presence of 100 nM Chetomin (C9623, Sigma) or DMSO (D8418, Sigma) control for 7 h before RNA preparation.

VEGFA ELISA assay. Cell culture medium of primary OPCs from Non-Cre control and *Cnp-Cre, Hif1α*fl/fl, *Hif2α*fl/fl were collected for VEGF measurement. Endogenous VEGF concentrations were determined using a mouse-specific VEGF Quantikine ELISA kit (t#MMV00, R&D System) according to the manufacture's instruction.

Transfection in primary OPCs and ELISA assay. Primary OPCs was transfected with Wls-ShRNA (TRCN 0000 234932, Mission ShRNA bacterial Glycerol stock
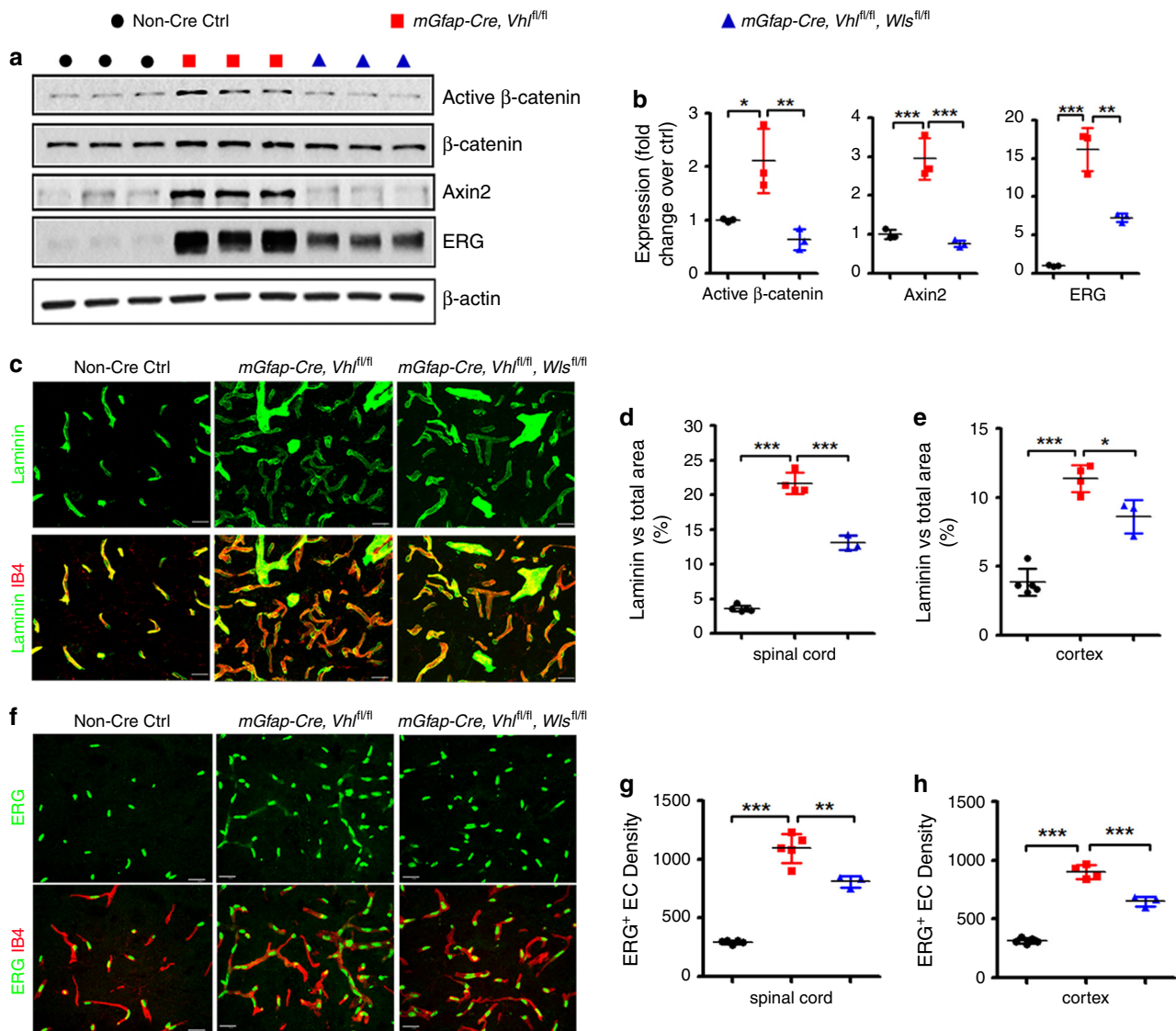
Fig. 9 Constitutively blocking Wnt secretion from astrocytes reduces HIFα-regulated angiogenesis in the early adult CNS. a, b Western blot (**a**) and quantification (**b**) of the active form of β-catenin, Wnt/β-catenin target gene Axin2, EC-specific nuclear protein ERG in the spinal cord at P30. One-way ANOVA followed by Tukey's multiple comparisons, *$P < 0.05$, **$P < 0.01$, ***$P < 0.001$. $F_{(2,6)} = 13.38$, $P = 0.0061$ active β-catenin, $F_{(2,6)} = 41.26$, $P = 0.0003$ Axin2, $F_{(2,6)} = 65.59$, $P < 0.0001$ ERG. n = 3 each group. **c** Representative confocal images of Laminin and IB4 in the spinal cord at P30, scale bars = 20 μm. **d, e** percentage of Laminin-occupying area among total area at P30. One-way ANOVA followed by Tukey's multiple comparisons, *$P < 0.05$, ***$P < 0.001$. $F_{(2,9)} = 332.0$, $P < 0.0001$ spinal cord, $F_{(2,9)} = 59.19$, $P < 0.0001$ cerebral cortex. $n = 5$ Ctrl, 4 VHL cKO, 3 VHL/WLS cKO. **f** Representative confocal images of ERG and IB4 in the spinal cord at P30, scale bars = 20 μm. **g, h** Densities (per mm^2) of ERG$^+$ ECs at P30. One-way ANOVA followed by Tukey's multiple comparisons, **$P < 0.01$, ***$P < 0.001$. $F_{(2,10)} = 124.1$, $P < 0.0001$ spinal cord, $F_{(2,9)} = 219.2$, $P < 0.0001$ cerebral cortex. $n = 5$ Ctrl, 5 VHL cKO, 3 VHL/WLS cKO. Data are shown as mean ± s.d. Source data of **a, b, d, e, g, h** are provided as a Source Data file.

NM_026582) and ShRNA scramble control (Mission TRC2 PlkO.5-PURO Non-Mammalian shRNA control Plasmid), Wnt7a plasmid pLCN-Wnt7a-HA (Addgene, #18036) and empty pLCN-exp (Addgene, #64865) at the time points indicated in Fig. 3a. The transfection was done by using FuGENE6 Transfection reagent (Promega, #E2691, lot#000371257). The Wnt7a in OPCs cell medium was measured by using mouse Wnt7a ELISA kit (Cusabio, #CSB-EL026141MO, Lot#G19147708) according to the manual of the kit.

Immunohistochemistry and blood vessel quantification. Study mice were perfused with ice-cold phosphate buffered saline (PBS, pH = 7.0, Catalog #BP399-20, Fisher Chemical), and then post-fix in fresh 4% paraformaldehyde (PFA, Catalog #1570-S, Electron Microscopy Science,PA) at room temperature(RT) for 2 h. The CNS tissue was washed in ice-cold PBS for three times, 15 min each time. The samples were cryoprotected with 30% sucrose in PBS (Sucrose, Catalog #S5-3, Fisher Chemical) for 20 h followed by sectioning. Sixteen microns thick sections were serially collected and stored in −80 °C. Immunohistochemistry was conducted as below: slices were air dry in RT for at least 1 h, and then were blocked

with 10% Donkey (Dky) serum for 1 h at RT. Tissue was incubated with primary antibody overnight at 4 °C. Slices were washed for 15 min in PBST (PBS with 0.1% Tween-20) for three times, then incubated with fluorescence conjugated secondary antibody (1:500; Alexa-fluorescence from Jackson ImmunoResearch) for 1.5 h at RT. Slices were washed 15 min in PBST (PBS with 0.1% Tween-20) for three times. The immunostaining was done before incubating with DAPI nuclear staining for 10 min[56,57]. The information of primary antibodies used for immunohistochemistry in the study were listed in Supplementary Table 1. For BrdU immunostaining, sections were pretreated with fresh-made 2N HCl (#320331, Sigma) followed by the above immunostaining procedures.

To quantify blood vessel density, we used projected confocal images at 40x magnification (Nikon C1) followed by NIH ImageJ automated processing. At least three sections from each mouse were used for ImageJ quantification. Ten-micron-thick optical sections from confocal z-stack images were projected into a flattened image. The parameter setting of z-stack confocal imaging is below: total optical thickness, 10 μm, step size, 0.5 μm, total number optical slices, 21. The volume-rendered confocal images were subsequently imported to NIH ImageJ 1.46r for quantifying Laminin-positive blood vessel density using a customer-defined Macro
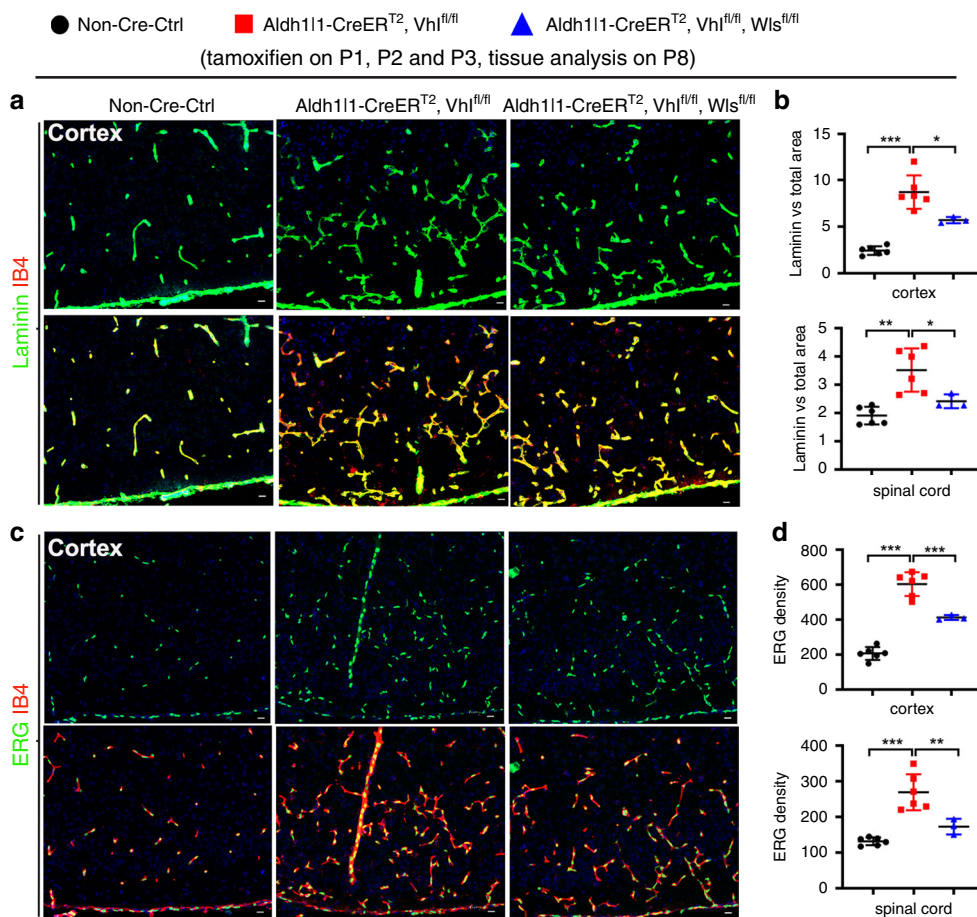
Fig. 10 Conditionally blocking Wnt secretion from neonatal astrocytes reduces HIFα-regulated CNS angiogenesis in the early postnatal CNS. a Representative confocal images of Laminin and IB4 in the cerebral cortex of each group of mice at P8 that had been treated with tamoxifen at P1, P2, and P3. **b** Percentage of Laminin-occupying area among the total area at P8. Cortex, one-way ANOVA followed by Tukey's multiple comparisons, *$P < 0.05$, ***$P < 0.001$, $F_{(2,12)} = 41.00$, $P < 0.0001$. Spinal cord, Welch's ANOVA followed by unpaired t test with Welch's correction, *$P < 0.05$, **$P < 0.01$ $W_{(2,6.824)} = 11.42$, $P = 0.0067$. $n = 6$ Ctrl, 6 VHL cKO, 3 VHL/Wls cKO. **c** Representative confocal images of ERG and IB4 in the P8 cerebral cortex of each group of mice that had been treated with tamoxifen at P1, P2, and P3. **d** Density (#/mm²) of ERG⁺ ECs at P8. One-way ANOVA followed by Tukey's multiple comparisons, **$P < 0.01$, ***$P < 0.001$. $F_{(2,12)} = 92.24$, $P < 0.0001$ cortex, $F_{(2,12)} = 24.37$, $P < 0.0001$ spinal cord. $n = 6$ Ctrl, 6 VHL cKO, 3 VHL/Wls cKO. Data are shown as mean ± s.d. Source data of **b**, **d** are provided as a Source Data file.

program. The total area and Laminin-occupying area were derived and from ImageJ and exported to Microsoft Excel for calculating the percent of Laminin-occupying area among assessed total CNS area.

mRNA In Situ hybridization (ISH). We employed the PCR and in vitro transcription to prepare cRNA probes targeting Vegfa and Plp[58]. Targeted sequences of Vegfa and Plp were generated by PCR. The primers used were: *Vegfa*-Forward: GGATATGTTTGACTGCTGTGGA; *Vegfa*-Reverse: AGGGAAGATGAGGAA GGGTAAG; *Plp*-Forward: GGGGATGCCTGAGAAGGT; *Plp*-Reverse: TGTGA TGCTTTCTGCCCA. We added the T7 (GCGTAATACGACTCACTATAGGG) and SP6 (GCGATTTAGGTGACACTATAG) promoter sequences to the 5' of the forward and reverse primers, respective. The SP6 and T7 promoter sequences are recognized by the SP6 and T7 RNA polymerase, respectively, in the subsequence in vitro transcription. PCR products of Vegfa and Plp amplification were used as DNA templates to transcribe into Vegfa and Plp cRNA probes in vitro using SP6 RNA polymerase. T7 RNA polymerase-mediated transcription of RNA was used as negative control. DIG-UTP or FITC-UTP was used to generate DIG- or FITC-labeled cRNA probes.

Single or dual mRNA ISH was done using our previous protocols[58]. Frozen sections of 14 μm thickness were used. The concentration of cRNA probe we used was 100 ng/100 μl hybridization buffer. Hybridization was conducted at 65 °C for 18–20 h. After hybridization, sections were treated with 10 μg/ml RNase A to eliminate nonspecific cRNA binding. For single mRNA ISH with DIG-labeled cRNA probes, DIG was recognized by alkaline phosphatase (AP)-conjugated anti-DIG (#11093274910, Sigma) antibody and DIG signals were visualized by the NBT/BCIP (#72091, Sigma) method. For dual fluorescence mRNA ISH (Vegfa and Plp), FITC-labeled Plp cRNA probe and DIG-labeled Vegfa cRNA probe were applied to frozen sections simultaneously during the hybridization step. The FITC signals

were visualized by tyramide signal amplification (TSA) fluorescence system (#NEL747A, Perkin Elmer) according to the manufacturer's instructions using horseradish peroxidase (HRP)-IgG Fraction Monoclonal Mouse Anti-Fluorescein (#200-032-037, Jackson ImmunoResearch). DIG signals were visualized by a HNPP fluorescent kit (#11758888001, Sigma) according to the manufacturer's instructions using AP-conjugated anti-DIG Fab² antibody (#11093274910, Sigma).

Western blot. Protein concentration was assessed by BCA protein assay kit (#23225, Thermo Fisher Scientific). Twenty microgram protein lysates were separated on AnykD Mini-PROTEAN TGX precast gels (#4569035, BIO-RAD) or 10% Mini-PROTEAN TGX precast gels (#4561035, BIO-RAD). The proteins were transferred onto 0.2 μm nitrocellulose membrane (#1704158, BIO-RAD) by Transblot Turbo Transfer system (#1704150, BIO-RAD). The membranes were blocked with 5% BSA (#9998, Cell signaling) for 1h at room temperature and were incubated overnight with primary antibodies (Supplementary Table 2) at 4 °C. The membranes were washed 3 times with 10 mm Tris-HCl (pH 7.5) containing 150 mM NaCl and 0.1% Tween-20 (TBST) and were incubated with horseradish peroxidase-conjugated goat anti-rabbit (31460, RRID: AB_228341, Thermo Fisher Scientific) or anti-mouse (31430, RRID: AB_228307, Thermo Fisher Scientific) for 1h at room temperature. After incubation, the membranes were washed three times with TBST. Specific binding was detected using Western Lightening Plus ECL (NEL103001EA, Perkin Elmer). NIH Image J 1.44p was used to quantify protein expression levels by analyzing the scanned grey-scale films.

RNA preparation and RT-qPCR. Total RNA was extracted by using Qiagen RNeasy for lipid tissues (74804, Qiagen) with additional on-column DNase I digestion to remove genomic DNA contamination. The quality and quantity of

RNAs were analyzed by the Nanodrop one^C microvolume UV-Vis Spectro-photometer (ND-ONEC-W, Thermo Fisher Scientific). cDNA was synthesized by Qiagen Omniscript RT Kit (205111, Qiagen). The relative mRNA level of indicated genes was normalized to that of the internal control Hsp90 and calculated by the equation $2^{\wedge(Ct(\text{cycle threshold}) \text{ of } Hsp90 - Ct \text{ of indicated genes})}$. The gene expression levels in control groups were normalized to 1. RT-qPCR was conducted by QuantiTect SYBR® Green PCR Kit (204145, QIAGEN) approaches on Agilent MP3005P thermocycler. The qPCR primers used in the study were listed in Supplementary Table 3.

Statistical analyses. Quantification was performed by blinded observers. All measurements were taken from distinct mice and quantitative data are presented as means ± standard deviation (s.d.). We used scatter dot plots to present the quantification data throughout our manuscript. Each dot (circle, square, or triangle) in the scatter dot plots represents one mouse or one independent experiment. Shapiro–Wilk approach was used for testing data normality. F test was used to compare the equality of variances of two groups whereas Browne–Forsythe test was used for comparing the equality of variances of three or more groups. The statistical methods were described in the figure legends and P value was presented in each graph. For unpaired, two-tailed Student's t test, t value and degree of freedom (df) were presented as $t_{(df)}$ in figure legends. Welch's correction was used for Student's t test if the variances of two groups were unequal after Browne–Forsythe test. For comparisons among three or more groups with equal variances (tested by Browne–Forsythe approach), ordinary one-way ANOVA was used followed by Tukey's multiple comparisons, otherwise Welch's ANOVA was used followed by unpaired t test with Welch's correction. In ordinary ANOVA, the F ratio and DFn and DFd was presented as $F_{(DFn, DFd)}$ in the figure legends where DFn stands for degree of freedom numerator and DFd for degree of freedom of denominator. In Welch's ANOVA, the Welch's F ratio, W and DFn and DFd was presented as $W_{(DFn, DFd)}$ in the figure legends. All data plotting and statistical analyses were performed using GraphPad Prism version 8.0. P value less than 0.05 was considered as significant, whereas greater than 0.05 was assigned as not significant (ns).

Reporting summary. Further information on research design is available in the Nature Research Reporting Summary linked to this article.

Data availability
The source data underlying Figs. 1b, c, e–m, 2a–k, 3b–d, 4c–f, h, j, k, l, 5c–f, 6a–c, f–i, 7a–g, 8c, d, f–g, 9a, b, d, e, g, h, 10b, d, Supplementary Figs. 3b–d, 4c, f, g, 6b, 7b, 8a, b, 9b, c, 10a–d, 11b, 12b, c, e, f, 13b are provided as a Source Data file. The data that support this study are available from the corresponding author upon reasonable request.

References
1. Harb, R., Whiteus, C., Freitas, C. & Grutzendler, J. In vivo imaging of cerebral microvascular plasticity from birth to death. *J. Cereb. Blood Flow. Metab.* **33**, 146–156 (2013).
2. Paredes, I., Himmels, P. & Ruiz de Almodovar, C. Neurovascular communication during CNS development. *Dev. Cell* **45**, 10–32 (2018).
3. Xiong, Y., Mahmood, A. & Chopp, M. Angiogenesis, neurogenesis and brain recovery of function following injury. *Curr. Opin. Investig. Drugs* **11**, 298–308 (2010).
4. Vallon, M., Chang, J., Zhang, H. & Kuo, C. J. Developmental and pathological angiogenesis in the central nervous system. *Cell Mol. Life Sci.* **71**, 3489–3506 (2014).
5. Ivanovic, Z. Hypoxia or in situ normoxia: the stem cell paradigm. *J. Cell Physiol.* **219**, 271–275 (2009).
6. Dengler, V. L., Galbraith, M. & Espinosa, J. M. Transcriptional regulation by hypoxia inducible factors. *Crit. Rev. Biochem Mol. Biol.* **49**, 1–15 (2014).
7. Semenza, G. L. Hypoxia-inducible factors in physiology and medicine. *Cell* **148**, 399–408 (2012).
8. Tomita, S. et al. Defective brain development in mice lacking the Hif-1alpha gene in neural cells. *Mol. Cell Biol.* **23**, 6739–6749 (2003).
9. Yuen, T. J. et al. Oligodendrocyte-Encoded HIF Function Couples Postnatal Myelination and White Matter Angiogenesis. *Cell* **158**, 383–396 (2014).
10. Guo, F. et al. Canonical Wnt signaling in the oligodendroglial lineage-puzzles remain. *Glia*, https://doi.org/10.1002/glia.22813 (2015).
11. Lappe-Siefke, C. et al. Disruption of Cnp1 uncouples oligodendroglial functions in axonal support and myelination. *Nat. Genet* **33**, 366–374 (2003).
12. Lang, J. et al. Adenomatous polyposis coli regulates oligodendroglial development. *J. Neurosci.* **33**, 3113–3130 (2013).
13. Tognatta, R. et al. Transient Cnp expression by early progenitors causes Cre-Lox-based reporter lines to map profoundly different fates. *Glia* **65**, 342–359 (2017).
14. Hammond, E. et al. The Wnt effector transcription factor 7-like 2 positively regulates oligodendrocyte differentiation in a manner independent of Wnt/beta-catenin signaling. *J. Neurosci.* **35**, 5007–5022 (2015).
15. Viziteu, E. et al. Chetomin, targeting HIF-1 alpha/p300 complex, exhibits antitumour activity in multiple myeloma. *Br. J. Cancer* **114**, 519–523 (2016).
16. Banziger, C. et al. Wntless, a conserved membrane protein dedicated to the secretion of Wnt proteins from signaling cells. *Cell* **125**, 509–522 (2006).
17. Bartscherer, K., Pelte, N., Ingelfinger, D. & Boutros, M. Secretion of Wnt ligands requires Evi, a conserved transmembrane protein. *Cell* **125**, 523–533 (2006).
18. Carpenter, A. C., Rao, S., Wells, J. M., Campbell, K. & Lang, R. A. Generation of mice with a conditional null allele for Wntless. *Genesis* **48**, 554–558 (2010).
19. Carpenter, A. C. et al. Wnt ligands from the embryonic surface ectoderm regulate 'bimetallic strip' optic cup morphogenesis in mouse. *Development* **142**, 972–982 (2015).
20. Zhang, Y. et al. An RNA-sequencing transcriptome and splicing database of glia, neurons, and vascular cells of the cerebral cortex. *J. Neurosci.* **34**, 11929–11947 (2014).
21. Reemst, K., Noctor, S. C., Lucassen, P. J. & Hol, E. M. The indispensable roles of microglia and astrocytes during brain development. *Front Hum. Neurosci.* **10**, 566 (2016).
22. Ma, S. & Huang, Z. Neural regulation of CNS angiogenesis during development. *Front Biol. (Beijing)* **10**, 61–73 (2015).
23. Chen, D. et al. HIF-1alpha inhibits Wnt signaling pathway by activating Sost expression in osteoblasts. *PLoS ONE* **8**, e65940 (2013).
24. Mazumdar, J. et al. O2 regulates stem cells through Wnt/beta-catenin signalling. *Nat. Cell Biol.* **12**, 1007–1013 (2010).
25. Kaidi, A., Williams, A. C. & Paraskeva, C. Interaction between beta-catenin and HIF-1 promotes cellular adaptation to hypoxia. *Nat. Cell Biol.* **9**, 210–217 (2007).
26. Majmundar, A. J. et al. HIF modulation of Wnt signaling regulates skeletal myogenesis in vivo. *Development* **142**, 2405–2412 (2015).
27. Santoyo-Ramos, P., Likhatcheva, M., Garcia-Zepeda, E. A., Castaneda-Patlan, M. C. & Robles-Flores, M. Hypoxia-inducible factors modulate the stemness and malignancy of colon cancer cells by playing opposite roles in canonical Wnt signaling. *PLoS ONE* **9**, e112580 (2014).
28. Zhong, Z. et al. Wntless functions in mature osteoblasts to regulate bone mass. *Proc. Natl Acad. Sci. USA* **109**, E2197–E2204 (2012).
29. Olsen, J. J. et al. The role of Wnt signalling in angiogenesis. *Clin. Biochem Rev.* **38**, 131–142 (2017).
30. Rosenstein, J. M., Krum, J. M. & Ruhrberg, C. VEGF in the nervous system. *Organogenesis* **6**, 107–114 (2010).
31. Mancuso, M. R., Kuhnert, F. & Kuo, C. J. Developmental angiogenesis of the central nervous system. *Lymphat Res Biol.* **6**, 173–180 (2008).
32. Sondell, M., Sundler, F. & Kanje, M. Vascular endothelial growth factor is a neurotrophic factor which stimulates axonal outgrowth through the flk-1 receptor. *Eur. J. Neurosci.* **12**, 4243–4254 (2000).
33. Sondell, M., Lundborg, G. & Kanje, M. Vascular endothelial growth factor has neurotrophic activity and stimulates axonal outgrowth, enhancing cell survival and Schwann cell proliferation in the peripheral nervous system. *J. Neurosci.* **19**, 5731–5740 (1999).
34. Namiecinska, M., Marciniak, K. & Nowak, J. Z. VEGF as an angiogenic, neurotrophic, and neuroprotective factor. *Postepy Hig. Med Dosw (Online)* **59**, 573–583 (2005).
35. Sun, Y. et al. VEGF-induced neuroprotection, neurogenesis, and angiogenesis after focal cerebral ischemia. *J. Clin. Invest* **111**, 1843–1851 (2003).
36. Hayakawa, K. et al. Vascular endothelial growth factor regulates the migration of oligodendrocyte precursor cells. *J. Neurosci.* **31**, 10666–10670 (2011).
37. Arai, K. & Lo, E. H. An oligovascular niche: cerebral endothelial cells promote the survival and proliferation of oligodendrocyte precursor cells. *J. Neurosci.* **29**, 4351–4355 (2009).
38. Arai, K., Jin, G., Navaratna, D. & Lo, E. H. Brain angiogenesis in developmental and pathological processes: neurovascular injury and angiogenic recovery after stroke. *FEBS J.* **276**, 4644–4652 (2009).
39. Stone, J. et al. Development of retinal vasculature is mediated by hypoxia-induced vascular endothelial growth factor (VEGF) expression by neuroglia. *J. Neurosci.* **15**, 4738–4747 (1995).
40. Komatsu, D. E. & Hadjiargyrou, M. Activation of the transcription factor HIF-1 and its target genes, VEGF, HO-1, iNOS, during fracture repair. *Bone* **34**, 680–688 (2004).
41. Nordal, R. A., Nagy, A., Pintilie, M. & Wong, C. S. Hypoxia and hypoxia-inducible factor-1 target genes in central nervous system radiation injury: a

role for vascular endothelial growth factor. *Clin. Cancer Res.* **10**, 3342–3353 (2004).

42. Cheng, L., Yu, H., Yan, N., Lai, K. & Xiang, M. Hypoxia-inducible factor-1alpha target genes contribute to retinal neuroprotection. *Front Cell Neurosci.* **11**, 20 (2017).

43. Stefater, J. A. 3rd et al. Regulation of angiogenesis by a non-canonical Wnt-Flt1 pathway in myeloid cells. *Nature* **474**, 511–515 (2011).

44. Clifford, R. L., Deacon, K. & Knox, A. J. Novel regulation of vascular endothelial growth factor-A (VEGF-A) by transforming growth factor (beta)1: requirement for Smads, (beta)-CATENIN, AND GSK3(beta). *J. Biol. Chem.* **283**, 35337–35353 (2008).

45. Wu, C. et al. Wnt/beta-catenin coupled with HIF-1alpha/VEGF signaling pathways involved in galangin neurovascular unit protection from focal cerebral ischemia. *Sci. Rep.* **5**, 16151 (2015).

46. Fancy, S. P. et al. Axin2 as regulatory and therapeutic target in newborn brain injury and remyelination. *Nat. Neurosci.* **14**, 1009–1016 (2011).

47. Fancy, S. P. et al. Parallel states of pathological Wnt signaling in neonatal brain injury and colon cancer. *Nat Neurosci*, https://doi.org/10.1038/nn.3676nn.3676[pii] (2014).

48. Ye, F. et al. HDAC1 and HDAC2 regulate oligodendrocyte differentiation by disrupting the beta-catenin-TCF interaction. *Nat. Neurosci.* **12**, 829–838 (2009).

49. Feigenson, K., Reid, M., See, J., Crenshaw, E. B. 3rd & Grinspan, J. B. Wnt signaling is sufficient to perturb oligodendrocyte maturation. *Mol. Cell Neurosci.* **42**, 255–265 (2009).

50. Zeis, T., Graumann, U., Reynolds, R. & Schaeren-Wiemers, N. Normal-appearing white matter in multiple sclerosis is in a subtle balance between inflammation and neuroprotection. *Brain* **131**, 288–303 (2008).

51. Graumann, U., Reynolds, R., Steck, A. J. & Schaeren-Wiemers, N. Molecular changes in normal appearing white matter in multiple sclerosis are characteristic of neuroprotective mechanisms against hypoxic insult. *Brain Pathol.* **13**, 554–573 (2003).

52. Lassmann, H. et al. A new paraclinical CSF marker for hypoxia-like tissue damage in multiple sclerosis lesions. *Brain* **126**, 1347–1357 (2003).

53. Lassmann, H. Hypoxia-like tissue injury as a component of multiple sclerosis lesions. *J. Neurol. Sci.* **206**, 187–191 (2003).

54. Gerber, H. P. et al. VEGF is required for growth and survival in neonatal mice. *Development* **126**, 1149–1159 (1999).

55. Weidemann, A. et al. The glial cell response is an essential component of hypoxia-induced erythropoiesis in mice. *J. Clin. Invest* **119**, 3373–3383 (2009).

56. Zhang, S. et al. Sox2 is essential for oligodendroglial proliferation and differentiation during postnatal brain myelination and CNS remyelination. *J Neurosci*. https://doi.org/10.1523/JNEUROSCI.1291-17.2018 (2018).

57. Zhang, S. et al. The stem cell factor Sox2 Is a positive timer of oligodendrocyte development in the postnatal murine spinal cord. *Mol. Neurobiol*. https://doi.org/10.1007/s12035-018-1035-7 (2018).

58. Guo, F. et al. Disruption of NMDA receptors in oligodendroglial lineage cells does not alter their susceptibility to experimental autoimmune encephalomyelitis or their normal development. *J. Neurosci.* **32**, 639–645 (2012).

Author contributions

F.G. conceived the original idea, led the project, and wrote the paper. S.Z. and B.K. conceived the idea, designed and performed experiments, analyzed data, and wrote the paper. X.Z., X.G., Y.W., Z.L., P.P., K.F., and A.W. analyzed data and edit the paper. All the authors provided feedback and comments on the paper.

Competing interests

The authors declare no competing interests.

Additional information

Supplementary information is available for this paper at https://doi.org/10.1038/s41467-020-15656-4.

Correspondence and requests for materials should be addressed to F.G.

Peer review information *Nature Communications* thanks Robert Miller, and the other, anonymous, reviewer(s) for their contribution to the peer review of this work. Peer reviewer reports are available.

Reprints and permission information is available at http://www.nature.com/reprints

Publisher's note Springer Nature remains neutral with regard to jurisdictional claims in published maps and institutional affiliations.